



# HHS Public Access

Author manuscript

Neuroimage. Author manuscript; available in PMC 2016 October 01.

Published in final edited form as:

Neuroimage. 2015 October 1; 119: 89–102. doi:10.1016/j.neuroimage.2015.06.033.

## Multivariate combination of magnetization transfer, $T_2^*$ and $B_0$ orientation to study the myelo-architecture of the *in vivo* human cortex

G. Mangeat<sup>1,3</sup>, S. T. Govindarajan<sup>3</sup>, C. Mainero<sup>3,4</sup>, and J. Cohen-Adad<sup>1,2</sup>

<sup>1</sup>Institute of Biomedical Engineering, Polytechnique Montreal, Montreal, QC, Canada

<sup>2</sup>Functional Neuroimaging Unit, CRIUGM, Université de Montréal, Montreal, QC, Canada

<sup>3</sup>Athinoula A. Martinos Center for Biomedical Imaging, MGH, Charlestown, MA, USA

<sup>4</sup>Harvard Medical School, Boston, MA, USA

### Abstract

Recently,  $T_2^*$  imaging at 7 tesla (T) MRI was shown to reveal microstructural features of the cortical myeloarchitecture thanks to an increase in contrast-to-noise ratio. However, several confounds hamper the specificity of  $T_2^*$  measures (iron content, blood vessels, tissues orientation). Another metric, magnetization transfer ratio (MTR), is known to also be sensitive to myelin content and thus would be an excellent complementary measure because its underlying contrast mechanisms are different than that from  $T_2^*$ . The goal of this study was thus to combine MTR and  $T_2^*$  using multivariate statistics in order to gain insights into cortical myelin content.

Seven healthy subjects were scanned at 7T and 3T to obtain  $T_2^*$  and MTR data, respectively. A multivariate myelin estimation model (MMEM) was developed, and consists in (i) normalizing  $T_2^*$  and MTR values and (ii) extracting their shared information using independent component analysis (ICA).  $B_0$  orientation dependence and cortical thickness were also computed and included in the model.

Results showed high correlation between MTR and  $T_2^*$  in the whole cortex ( $r=0.76$ ,  $p<10^{-16}$ ), suggesting that both metrics are partly driven by a common source of contrast, here assumed to be the myelin. Average MTR and  $T_2^*$  were respectively  $31.0 \pm 0.3\%$  and  $32.1 \pm 1.4$  ms. Results of the MMEM spatial distribution showed similar trends to that from histological work stained for myelin ( $r=0.77$ ,  $p<0.01$ ). Significant right-left differences were detected in the primary motor cortex ( $p<0.05$ ), the posterior cingulate cortex ( $p<0.05$ ) and the visual cortex ( $p<0.05$ ).

This study demonstrates that MTR and  $T_2^*$  are highly correlated in the cortex. The combination of MTR,  $T_2^*$ , CT and  $B_0$  orientation may be a useful means to study cortical myeloarchitecture with

---

**Corresponding author:** Julien Cohen-Adad, Ph.D., Institute of biomedical engineering, Polytechnique Montreal, Campus Université de Montréal, 2900 Edouard-Montpetit Bld, Montreal, QC, H3T1J4, Canada. Tel: 514-340-4711; Fax: 514-340-4611; jcohen@polymtl.ca.

**Publisher's Disclaimer:** This is a PDF file of an unedited manuscript that has been accepted for publication. As a service to our customers we are providing this early version of the manuscript. The manuscript will undergo copyediting, typesetting, and review of the resulting proof before it is published in its final citable form. Please note that during the production process errors may be discovered which could affect the content, and all legal disclaimers that apply to the journal pertain.

more specificity than using any of the individual methods. The MMEM framework is extendable to other contrasts such as T1 and diffusion MRI.

## Keywords

MTR;  $T_2^*$ ; B0 orientation; myeloarchitecture; ICA; Brodmann

## Introduction

Myeloarchitecture refers to the spatial organization of myelinated fiber in the central nervous system, including features such as their size, density orientation, and myelination (Flechsig, 1920; Vogt, 1911). The study of myeloarchitecture in the *in vivo* human cortex can provide further elements about the organization of the healthy and pathological cortex.

Previous studies have shown that  $T_2^*$  magnitude and phase images can reveal exquisite details of cortical microstructure, with enhanced contrast at ultra-high field strength (Duyn et al., 2007; Li et al., 2009, 2006).  $T_2^*$  is the effective transverse relaxation and is driven by microscopic and macroscopic field inhomogeneities, e.g. caused by susceptibility differences between tissues (Cohen-Adad, 2014). Of interest,  $T_2^*$  contrast is notably influenced by the size, density and orientation of myelinated fibers (Hwang et al., 2010; Lee et al., 2012; Pitt et al., 2010). Surface-based analysis of  $T_2^*$  revealed several features that correlate with myelin distribution in the cortex (Cohen-Adad et al., 2012, 2011; Deistung et al., 2013; Mainero et al., 2015). Similar observations were obtained from  $T_1$  (Dinse et al., 2013) and  $T_1w/T_2w$  (Glasser and Van Essen, 2011) measurements, further confirming the influence of myelin on  $T_2^*$  contrast. Despite its sensitivity to myeloarchitecture,  $T_2^*$  it is influenced by several confounds, such as the tissues iron level (Fukunaga et al., 2010), B0 field inhomogeneities (Hernando et al., 2012) and fibers orientation with respect to B0 (Cohen-Adad et al., 2012). Hence, combining  $T_2^*$  with another measure sensitive to myelin would increase the confidence in assessing the degree of myelination, as has been shown *ex vivo* (Tardif et al., 2012).

Magnetization Transfer (MT) imaging was shown to be sensitive to myelin content (Levesque and Pike, 2009; Schmierer et al., 2004) in white matter (WM) and thus would be an excellent complementary measure because its underlying contrast mechanisms are different than that from  $T_2^*$ . The MT effect results from the interaction between two kinds of hydrogen nucleus: protons in a liquid state associated with water molecules and protons in semisolid state associated with macromolecules. The macromolecular spins can be saturated by an off-resonance radio frequency (RF) pulse because they have a much broader absorption lineshape than the liquid spins. The preferential saturation of the macromolecular spins can be transferred to the liquid spins, depending on the rate of exchange (Levesque and Pike, 2009). This water spin saturation can then be detected with MRI (Henkelman et al., 2001). MTR is an index calculated using images with and without MT saturation pulse and was shown to correlate with myelin content (Henkelman et al., 2001; Schmierer et al., 2004). Recently, MTR was mapped in the cortex of MS patients (Chen et al., 2013; Derakhshan et al., 2014) and showed similarities between myelinated regions and high MTR

values. However, MTR is only a semi-quantitative metric as it depends on sequence parameters, B1 profile and T1 relaxation (Berry et al., 1999; Pike Bruce, 1996).

Combining MTR with T<sub>2</sub>\* thus appears to be a useful means to gain insight into cortical myelination because these two metrics are sensitive to myelin content but are based on different biophysical phenomena. MTR increases with myelin and T<sub>2</sub>\* decreases with myelin.

However, mapping T<sub>2</sub>\* and MTR in the cortex is challenging because the cortical ribbon is thin, highly convoluted and its geometry varies across individuals. Cortical surface-based analysis allows robust visualization of MRI measurements across the entire cortex and enables the calculation of spatial statistics at a population scale (Dale et al., 1999; Derakhshan et al., 2014; Fischl, 2012; Fischl et al., 1999; Glasser and Van Essen, 2011). Other confounds exist that can affect cortical mapping studies. Namely, (i) the effect of cortical thickness, which can introduce variable amount of partial volume effect and (ii) the angle between coherently-oriented myelinated fibers in the cortex and the direction of the main magnetic field (B<sub>0</sub>) (Cohen-Adad et al., 2012). Multivariate statistics, such as Independent Component Analysis (ICA) can decompose multivariate signal into independent signals coming from independent sources (Bingham and Hyvärinen, 2000; Hyvärinen and Oja, 2000; Xie and Wu, 2006). Here, ICA would be an adequate candidate for probing the existence of shared information between T<sub>2</sub>\*- and MTR-derived signal related to myelin content, while taking into account confounding factors (thickness, B<sub>0</sub> orientation).

The goals of the present study were: (i) to map T<sub>2</sub>\* at 7T and MTR at 3T in the healthy *in vivo* human cortex using surface-based analysis and (ii) to combine T<sub>2</sub>\* and MTR using a multivariate model in order to extract the shared information related to myelin.

## Material and Methods

### A. Data acquisition

Healthy subjects (N=7, gender = 4F and 3M, age = 36 +/- 5 years) were recruited. Subjects were scanned with a 7T whole-body scanner (Siemens Healthcare, Erlangen, Germany) to measure T<sub>2</sub>\* and with a 3T scanner (Siemens TIM Trio) to measure MTR. We chose not to perform the MTR protocol at 7T due to the less homogeneous B1 profile and SAR limitations. Both scanners were equipped with a 32-channel coil. Parameters values at 7T were: 2D gradient-echo, TR = 2020 ms, TE = 6.34+3.2n [n=0,...,11] ms, resolution = 0.33×0.33×1 mm<sup>3</sup>, acquisition time (TA) was 20 min (10 min/slab \* 2 slab). Parameters for the 3T magnetization transfer contrast were: Spoiled gradient echo sequence: 3D FLASH (Fast Low-Angle Shot), TR/TE = 30/2.49 ms, matrix = 192×192, resolution = 1.2×1.2×1.2 mm<sup>3</sup>, with (*mt\_on*) and without (*mt\_off*) MT pulse. The MT pulse is a Gaussian envelope with pulse duration = 9984μs and frequency offset = 1200 Hz. The acquisition time (TA) of each FLASH volume was 7:45 min. In addition to the MTR protocol, a T1-weighted image was acquired at 3T for cortical surface reconstruction using a magnetization-prepared rapid acquisition with multiple gradient echoes (MEMPR) (van der Kouwe et al., 2008). Parameters were: TR/TI=2530/1200 ms, TE=[1.7, 3.6, 5.4, 7.3] ms, flip angle (α)=7°,

FOV=230×230 mm<sup>2</sup>, resolution=0.9×0.9×0.9 mm<sup>3</sup>, bandwidth=651 Hz/pixel, scan time=6.5min. The reason for doing surface reconstruction from 3T data is that this protocol has been thoroughly validated (Dale et al., 1999; Govindarajan et al., 2014; Postelnicu et al., 2009; van der Kouwe et al., 2008), in comparison with the 7T MEMPR protocol, from which the less homogeneous B1+ profile can produce errors in segmentations.

## B. Data processing

Figure 1 shows an overview of the data processing pipeline. Pre-processing steps included: (i) computing MTR and T<sub>2</sub>\*. (ii) registering MTR and T<sub>2</sub>\* volumes to the cortical surface model, (iii) sampling the obtained values within the cortex, (iv) calculate the cortical thickness and (v) computing the angle between B0 field and the vector normal to the cortical surface. Processing was done with FreeSurfer (<http://surfer.nmr.mgh.harvard.edu>) and custom-made scripts written in MATLAB.

T<sub>2</sub>\* data were first corrected for background inhomogeneities as described in (Cohen-Adad et al., 2012), then T<sub>2</sub>\* was estimated using monoexponential fitting. A gross alignment was first performed between the averaged first 4 echoes of the T<sub>2</sub>\*-weighted volume and the T<sub>1</sub>weighted volume (at 3T) following the protocol described in (Govindarajan et al., 2014). Then, a fine alignment of the T<sub>2</sub>\*-weighted volume to the surface was estimated using the boundary-based registration method (BBR, 9 degrees of freedom), which is based on the local intensity gradient and was shown to have high robustness and accuracy (Greve and Fischl, 2009). Then, the registration matrices were applied to the T<sub>2</sub>\* volume. More details can be found in (Cohen-Adad, 2014). All registrations were visually inspected. For pre-processing of MTR data, both volumes with (*mt\_on*) and without (*mt\_off*) the Gaussian MT pulse were registered to the 3T T<sub>1</sub>-weighted volume using the function *mri\_robust\_register* available in FreeSurfer (Reuter et al., 2010). The *mt\_off* volume was registered to the surface using *bbregister* (12 d.o.f.). The resulting affine matrix was then applied to the MTR volume. Once both *mt\_on* and *mt\_off* were registered to the cortical surface, MTR was computed as follows:

$$MTR=100 * \frac{mt\_off - mt\_on}{mt\_off} \quad (1)$$

Figure 1 shows the MTR registrations steps. Once registered to the individual surface, MTR and T<sub>2</sub>\* were sampled at the mid distance between the pial and the white matter surface (50% depth) as done in (Cohen-Adad, 2014). The mid-cortical distance was chosen in order to minimize partial volume effect. Cortical thickness (CT) map was calculated using the normal distance between both pial and white matter surfaces previously segmented by *freesurfer*. B0 orientation dependence was estimated using the angle  $\theta_z$  between the normal vector of the surface and the B0 field direction (Cohen-Adad et al., 2012). MTR, T<sub>2</sub>\*, CT and B0 orientation data were then spatially normalized to the existing common space (*fsaverage*) available in FreeSurfer V4.2. Spatial normalization was performed using a spherical averaging procedure as described in (Fischl et al., 1999). For each subject, the cortical manifold was projected onto the target surface (*fsaverage*) and assigned a normal vector field with a consistent orientation.

Mean and inter-subject standard deviation (SD) maps were calculated for MTR,  $T_2^*$ , CT and B0 orientation. Then, Pearson's coefficient was calculated vertex-wise between each pair of the following parameters: MTR,  $T_2^*$ , CT and B0 orientation.

### C. Multivariate Myelin Estimation Model (MMEM)

Here we propose a method to merge the myelin-related information contained in MTR and  $T_2^*$  into a single metric. The framework works as follows: Firstly, multilinear regressions were performed using predictors of myelin content (MTR and  $T_2^*$ ) and confounding covariates (cortical thickness, which can introduce variable amount of partial volume effect, and B0 orientation dependency). Secondly, independent component analysis (ICA) is used to combine MTR- and  $T_2^*$ -derived signal related to myelin.

The detailed steps of the MMEM are represented in Figure 2. Firstly, two maps were estimated using multilinear regressions: one using the regressors MTR, CT and B0 orientation (ME\_MTR) and one using the regressors  $T_2^*$ , CT and B0 orientation (ME\_ $T_2^*$ ). ME\_MTR and ME\_ $T_2^*$  maps respectively represent MTR and  $T_2^*$  values corrected for partial volume effect and fibers orientation. Notice that constant regressors such as age and gender were in the constant term of the regression because the MMEM was performed independently for each subjects and the resulting map was normalized under a common dynamic range (explained below). ME\_MTR and ME\_ $T_2^*$  maps were calculated using equations (2) and (3):

$$ME\_MTR = a_1 + b_1 MTR + c_1 CT + d_1 \sin(2\theta_z) + e_1 \cos(2\theta_z) \quad (2)$$

$$ME\_T_2^* = a_2 + b_2 T_2^* + c_2 CT + d_2 \sin(2\theta_z) + e_2 \cos(2\theta_z) \quad (3)$$

where  $a$ ,  $b$ ,  $c$ ,  $d$  and  $e$  are the resulting parameters of the multilinear regressions.  $\theta_z$  is the angle between the surface's normal vector and the B0 magnetic field direction. The estimation of B0 orientation dependency was based on the model presented in (Cohen-Adad et al., 2012; Lee et al., 2011) but rearranged in a linear form to be used in a linear regression. More specifically, the sine function from the orientation dependency model was broken down into a linear sum of sine and cosine (see equation 1,2 and Supplementary Material S1 for the whole derivation). In order to merge MTR and  $T_2^*$  within the same framework, both linear regressions were performed with a common dependent variable. This dependent variable was a binary map made of regions that are known to be highly (BA1, BA4 and BA42) and poorly myelinated (BA8 and BA9) (Annese et al., 2004; Glasser and Van Essen, 2011; Glasser et al., 2014; Laule et al., 2008; Nieuwenhuys, 2013; Vogt, 1911). BA3 was not considered because of the thinness of the cortex in this region (mean CT=1.8mm) and hence strongly hampered by partial volume effect. The regions of high and low myelin content were arbitrarily set to 70% and 30%. It is however important to keep in mind that these arbitrary values were only chosen for adjusting the dynamics of both metrics (i.e. ME\_MTR and ME\_ $T_2^*$ ), on a subject-by-subject basis, in order to explore the relative distribution of myelin-related values throughout the entire cortical ribbon. Secondly, the shared information between ME\_MTR and ME\_ $T_2^*$  was extracted using ICA decomposition, for each subject. ICA was chosen because (i) it is an unsupervised data-

driven algorithm and is therefore free from arbitrary priors, (ii) it outputs mathematically independent components (as opposed to PCA) and (iii) the ‘so-called’ first component represents the shared information from ME\_MTR and ME\_T2\* with the highest variance, which is assumed to represent myelin. This assumption is based on previous studies demonstrating the sensitivity of T2\* and MTR to myelin content (Cohen-Adad et al., 2011; Deistung et al., 2013; Levesque and Pike, 2009; Mainero et al., 2015; Schmierer et al., 2004). The hypothesis being that the first component of the ICA was a more specific indicator for myelin content than a single metric taken separately. This hypothesis was further confirmed by simulations (see Supplementary Material S2) and comparison with previous histology works (Braitenberg 1962). The final multivariate myelin estimation was calculated from the principal independent vector of the ICA’s separating matrix ( $V_1$ ) and the matrix ( $X$ ) containing ME\_MTR and ME\_T2\* data (equation 4). This map was named Combined Myelin Estimation (*CME*).

$$CME = V_1^T * X \quad (4)$$

The robustness of the ICA decomposition was qualitatively checked for each subject by plotting the ICA’s vectors on the original set of data. The ICA’s first component map was then computed for each subject separately. Lastly, the ICA’s first component map were averaged across subjects.

The PALS-B12 Brodmann atlas (Van Essen, 2005) was used for interrogating sub-region of the cortex defined by their cyto-architecture. This choice was driven by previous studies showing homogenous myeloarchitecture within functional areas (Abdollahi et al., 2014; Bock et al., 2009; Geyer and Turner, 2013; Glasser and Van Essen, 2011; Glasser et al., 2014; Nieuwenhuys, 2013; Sereno, 1991).

## Results

### A. MTR, T<sub>2</sub>\*, CT and B0 orientation mapping

MT and T<sub>2</sub>\* data were successfully acquired in 6 out of 7 subjects. Visual inspection revealed excessive motion in one subject for the MT data. Hence only 6 subjects were used for subsequent analyses.

Figure 3A shows maps of 3T MTR, 7T T<sub>2</sub>\*, CT and B0 orientation averaged across subjects. MTR map shows high values (>32%) notably in the primary motor cortex (BA4), in the primary somatosensory cortex (BA1, BA2 & BA3), in the somatosensory association cortex (BA5 & BA7), in the posterior cingulate cortex (BA31 & BA23), in the visual cortex (BA17, BA18 & BA19) and in the auditory cortex (BA42). However, some ‘strip’ patterns of lower MTR are observed in these regions, notably in the central sulcus (~BA3) and in the calcarine fissure. The CT map also highlights a ‘strip’ pattern in BA3 and shows some regions of low cortical thickness (< 2mm) around the calcarine sulcus. These regions are also highlighted by the CT map by showing thin cortical thickness (between 1 and 2mm). In the frontal cortex MTR is notably low. T<sub>2</sub>\* map shows an overall similar pattern but with an opposite tendency. Low values (<25ms) are visible in the primary motor cortex, the primary

somatosensory cortex and in the visual cortex whereas  $T_2^*$  is high (~35ms) in the frontal lobe. The CT map shows lower cortical thickness in BA3, BA17 and BA18 as previously shown (Clarkson et al., 2011; Cohen-Adad et al., 2012).

Figure 3B shows maps of SD across subjects for the respective metrics. MTR SD is fairly homogenous and small in the whole cortex (~1.5%).  $T_2^*$  SD also exhibits fairly small values across the cortex (~2.5ms), however extreme values are found in the lower brain region, likely due to inhomogeneous B0 field at 7T. These fairly small SD maps for MTR and  $T_2^*$  suggest that the two metrics have centered and narrow distributions across subjects and hence the averaged maps are representative of the population studied here. Cortical thickness SD and B0 orientation SD were fairly large on a voxel-by-voxel basis (average SD was respectively 0.47mm and 17.4°), suggesting that there is an inter-subject variability in the morphology of the cortex, e.g., thickness, location and orientation of different gyri/sulci.

Table 1 summarizes the whole brain statistics (mean, inter subject SD and coefficient of variation (COV)). COV coefficients are calculated by performing the ratio between the inter-subjects SD and the mean across the whole cortex. COV are displayed percentage. Inter-subject SD and COV are fairly small for all metrics as previously seen on the maps.

### B. Pearson's correlations between MTR and $T_2^*$

Figure 4 shows the Pearson's correlations between MTR and  $T_2^*$ . Different colors are showing the vertices density in order to better visualize scatter's shape. To reduce the high-frequency noise in the correlation space (MTR vs.  $T_2^*$ ) a 2-dimensional smoothing of 10 points was achieved before computing the Pearson's correlation. Strong correlations were observed in the right ( $r=-0.77$ ) and left ( $r=-0.75$ ) hemispheres. The colormap reveals higher density in the center of the scatter showing a 2D Gaussian tendency well defined at the center of the distributions.

We also assessed the whole cortex correlation between  $T_2^*$  & CT ;  $T_2^*$  & B0 orientation ; MTR & CT and MTR & B0 orientation. Table 2 shows their corresponding Pearson's correlation coefficient. We can see that in the whole cortex, correlations with B0 orientation are fairly low.

### C. Distribution graph

The distribution graph (Figure 5) is a qualitative way to visualize spatial correlations between MTR,  $T_2^*$ , CT and B0 orientation for assessing the feasibility to combine these four metrics using a linear model (first step of the MMEM). First, we compared the shape of MTR,  $T_2^*$ , CT and B0 orientation across all 164,000 vertices. Vertices of the mean  $T_2^*$  map (in red) were sorted in the ascending order. The same index distribution was then used to display MTR (blue), CT (magenta) and B0 orientation (green) values. For clarity, values were smoothed along the abscissa (100-point window). Inter subjects SD have also been plotted for each vertex. We chose to sort  $T_2^*$  values instead of MTR due to the larger number of artefactual vertices in the  $T_2^*$  data, leading to extremely low or high values, related to field inhomogeneity and/or surface registration (Cohen-Adad, 2014). Only the right hemisphere values are plotted for more clarity. Similar trends are observed between left and right hemispheres.

In order to further explore the different trends between metrics, the distribution graph was divided into four ensembles of vertices:

- Region 1 (light blue on figure 5): Vertices hampered by strong artifacts on  $T_2^*$  data caused by signal dropout ( $T_2^* < 24\text{ms}$ ). This region contains less than 2% of all cortical vertices.
- Region 2 (dark blue): Vertices for which MTR and  $T_2^*$  are correlated. Interestingly, these vertices are mainly located in the gyri adjacent to the central sulcus and the calcarine fissure. There are some dark blue areas that neighbor light blue areas in the lower brain region, and these vertices are likely affected by artifacts due to poor shimming in this region. However, we believe that the same pattern observed in other vertices (e.g., visual and motor cortex) is genuine. This region contains less than 2% of all vertices.
- Region 3 (yellow): Vertices where MTR and  $T_2^*$  are anti-correlated (R-squared  $> 0.90$ ). This region contains more than 96% of all vertices.
- Region 4 (red): Vertices with high  $T_2^*$  values ( $> 40\text{ms}$ ), notably in anterior cingulate cortex (BA24 & BA32). These vertices are possibly affected by surface misregistration.

The main purpose of this graph was to identify vertices where a linear relationship between MTR and  $T_2^*$  can be tested without introducing too much bias. Based on these results, the combination into a unique framework for estimating myelin content (MMEM, see below) will be performed on region #3.

#### D. Multivariate myelin estimation model (MMEM)

**Multilinear regression**—Table 3 shows results of the linear models defined in Figure 2 and equations 2,3. These results show that myelin estimation is proportional to MTR and is inversely proportional to  $T_2^*$ , as was expected (Cohen-Adad et al., 2011; Schmierer et al., 2004). Secondly, we notice that MTR accounts for about 54% of the ME\_MTR metric and  $T_2^*$  accounts for about 38% of the ME\_  $T_2^*$  metric, whereas cortical thickness and B0 orientation have lesser influence (6% and  $< 1\%$ , respectively). Thirdly, we notice a fairly low inter-subject variability for the fittings coefficients of the constant part ( $a$ ), the MTR or  $T_2^*$  part ( $b$ ) and the cortical thickness part ( $c$ ), that suggest a fairly good robustness of the model. However we notice a high variability of  $d$  and  $e$  parameters. We believe this is related to the fact that even though  $T_2^*$  is modulated by B0 orientation with respect to cortical surface (Cohen-Adad et al., 2012), this modulation is fairly low compared to that in the white matter. Evidences are found in gray/white matter comparative studies from (Sati et al., 2012). Moreover, it is possible that there is an inter-subject variability in the morphology of the cortex, e.g., orientation of coherently-aligned cortical fibers. Again, our model is performed in a subject by subject basis, and thus is not affected by the morphological inter-subject variability.

**Independent Component Analysis (ICA)**—The second step was to perform an ICA for each subject, in order to find a transformation matrix that optimizes the extraction of the common information contained in ME\_MTR and ME\_  $T_2^*$  (Hyvärinen and Oja, 2000; Xie

and Wu, 2006). However, performing an ICA with large data vector (~164,000 vertices) is poorly robust. Therefore, a graphical validation of each ICA result (one per subject) was made. This graphical validation was useful to assess the result of each ICA's and the inter-subject consistency between results.

Figure 6A shows results of ICA for each subject. Pink arrows are the two vectors of the separating matrix  $W$  found by the ICA (Hyvärinen et al, 2000). Figure 6B represents the projection of the ME\_MTR and ME\_T<sub>2</sub>\* data into the space defined by the two vectors of the ICA's separating matrix. These graphs are useful to assess the non-correlation ( $r < 0.06$ ) of the resulting set of data.

The inter-subject variability of ICA results is fairly low (First vector direction =  $58 \pm 4^\circ$  and angle between both vectors =  $112 \pm 5^\circ$ ), justifying the relevance of computing an average map of principal components across subjects.

**Combined Myelin Estimation (CME)**—Figure 7 shows the average map of the Combined Myelin Estimation (CME). This map was computed from the first component of the ICA using equation (3) and averaged across subjects. The CME represents the common entity contained by ME\_MTR and ME\_T<sub>2</sub>\*, i.e., the source shared between ME\_MTR and ME\_T<sub>2</sub>\* that is mathematically independent from the rest of the acquired signal. Therefore, CME is thought to reflect the cortical myelin content with greater specificity than MTR or T<sub>2</sub>\* alone. The mean and SD of CME across the cortex was  $50.3 \pm 0.7$ . Overall, we notice a high myelin estimation (yellow/red) in the primary motor cortex BA4= $74 \pm 3\%$  (here, % refers to the CME metric, and  $\pm 3\%$  refers to the SD across subjects) and in the primary somatosensory cortex (BA1= $67 \pm 7\%$ , BA2= $59 \pm 4\%$  and BA3= $63 \pm 13\%$ ). Moreover, a high myelin estimation is also observed in the visual cortex (BA17= $67 \pm 5\%$  & BA18= $68 \pm 6\%$ ) and the auditory cortex (BA42= $57 \pm 10\%$ ). These results are consistent with previous study (Annese et al., 2004; Glasser and Van Essen, 2011; Glasser et al., 2014; Laule et al., 2008; Nieuwenhuys, 2013; Vogt, 1911).

**CME maps comparisons**—Figure 8A shows a side-by-side comparison of CME, ME\_MTR and ME\_T<sub>2</sub>\* on the inflated cortical surface. Major differences between ME\_MTR and ME\_T<sub>2</sub>\* are indicated with white circles (plain and dashed). In the medial view of ME\_T<sub>2</sub>\*, one can observe a higher signal in the visual cortex than that in the ME\_MTR (plain-circle). Inversely, the ME\_T<sub>2</sub>\* map shows a lower signal in the precuneus areas (small-dashed-circle) and superior frontal cortex (middle-dashed-circle) compared to that in the ME\_MTR map. In the lateral view of the ME\_MTR map, one can observe a higher signal in the somatosensory association cortex (small-dashed-circle) and in the angular gyrus (plain-circle), compared to that in the ME\_T<sub>2</sub>\* map. Figure 8B,C show correlations between the myelin estimations metrics and histology values from (Braitenberg 1962), which are based on optical attenuation measures in an ex vivo human cortex stained for myelin. The Pearson's correlation coefficients of: ME\_MTR vs. Histology, ME\_T<sub>2</sub>\* vs. Histology and CME vs. Histology, were respectively 0.71 (p-value < 0.05), 0.69 (p-value < 0.05) and 0.77 (p-value < 0.01). These correlations suggest that CME is a more specific marker for cortical myelin content than ME\_MTR or ME\_T<sub>2</sub>\* taken separately.

## E. Analyses within Brodmann Areas

Figure 9A shows the CME map with an overlay of the PALS-B12 Brodmann Areas (BA). This figure shows a fair adequation between variations of CME and BA borders, for instance in BA1, BA2, BA3 and BA4 (primary motor and primary somatosensory cortex, green arrows), in BA17, BA18, BA19 (visual cortex, blue arrows) and in BA42 (auditory cortex, yellow arrow). However, in several areas (for instance BA22 or BA39) CME is quite heterogeneous, suggesting to divide these regions in smaller areas if we aimed to build a more accurate myelo-architectural atlas.

Figure 9B shows the CME map averaged within each BA and Figure 9C shows the mean BA values, as well as the inter-subject SD and the intra-area SD. In comparison with the SD across the entire cortex (26.5%), the intra-area SD is fairly low (in average 11.9%). We also note that the inter-subject SD is low, with an average coefficient of variation of 25% (here the average COV was calculated by computing the COV for each area, and then averaging all COVs across areas).

Figure 10 shows bar graphs representing mean and intersubject SD values of the different metrics used in the model (CME, MTR, ME\_MTR,  $T_2^*$ , ME\_ $T_2^*$ ) within Brodmann regions. This graph shows the inter-hemispheric differences across (CME, MTR, ME\_MTR,  $T_2^*$  and ME\_ $T_2^*$ ). Overall, we observe a fairly good right-left reproducibility, except in some regions as described hereafter. The CME map shows significant hemispheric differences in BA4 and BA31 (more myelin estimated in RH,  $p < 0.05$ ) and in BA17 and BA23 (more myelin estimated in LH, respectively  $p < 0.05$  and  $p < 0.01$ ).

## Discussion

This study presented a novel approach to combine MTR and  $T_2^*$  in the *in vivo* human cortex, with the goal of studying cortical myeloarchitecture. We proposed to use a multivariate model to extract myelin-related information shared by both metrics. The model takes into account cortical thickness and B0 orientation and is flexible, i.e., other metrics such as T1 and diffusion data can be added. In the following, we discuss the sensitivity and specificity of MTR and  $T_2^*$  to detect myelin content, the multivariate model and ICA decomposition for combining MTR and  $T_2^*$  and the resulting maps, limitations and perspectives.

### Sensitivity and specificity of MTR and $T_2^*$ for quantifying myelin content

MT reflects the relative density of macromolecules, such as lipids or proteins. Since myelin has a lipid-protein structure (~80% lipids and ~20% protein), MT is able to provide indirect measure of myelin content. The MT phenomenon is complex and some of its underlying physical mechanisms are still unknown (Kim and Cercignani, 2014). Overall, the MT effect induces reduction of signal in tissues with large amount of MT, such as those with high concentration in macromolecules (e.g., lipids). For example, MT ratio (MTR) was shown to correlate well with myelin content in the white matter (Schmierer et al., 2004). Recently, MTR was shown to be sensitive to cortical demyelination in multiple sclerosis patients (Chen et al., 2013; Derakhshan et al., 2014). However, MTR is only a semi-quantitative

metric and has several confounds. Firstly, B1 inhomogeneities related to RF transmission induce variabilities on the MT pulse power, which affect MTR measures. Secondly, MTR values depend on the sequence parameters (Berry et al., 1999). Thirdly, MTR values are affected by T1 relaxation (Pike Bruce, 1996). Despite the longer acquisition time, quantitative MT (Levesque and Pike, 2009) provides more accurate estimation of myelin content.

T2\* is the effective transverse relaxation time and is therefore affected by (i) mesoscopic field inhomogeneities, which result from susceptibility differences between tissues (parenchyma, deoxygenated blood, bone, cartilage, etc.) and (ii) macroscopic field inhomogeneities, which arise from magnetic field imperfections, air-tissue boundaries, or ferromagnetic objects (e.g., metal clips, implants, dental prosthesis). The latter are characterized by large-scale gradients that cause enhanced signal decay in gradient echo images and thus apparent decrease in T2\* that can confound the underlying biology. Furthermore, the specificity of T2\* contrast to myelin content is hampered by fiber orientation in the white matter (Lee et al., 2011) and in the cortex (Cohen-Adad et al., 2012), tissue iron level (Lee et al., 2012; Stüber et al., 2014), blood vessels (Spees et al., 2001), blood oxygen level (Li et al., 1998). Note that in this study, the effect of blood vessel was minimized by excluding large blood vessels using manual masks. Also, capillary blood should only contribute minimally to the T2\* contrast, as reported by Lee et al. (Lee et al., 2012).

### Combining MTR and T<sub>2</sub>\* using ICA

The main goal of this study was to gain specificity in myelin mapping by combining T2\* and MTR. Here, ICA decomposition was chosen to extract shared information between MTR and T<sub>2</sub>\* that represents myelin content. The ICA offers the advantage of recovering sources of interest (here: myelin content) from observed mixtures, making it well suited for the brain data analysis because of the multifaceted origin of MTR and T<sub>2</sub>\* contrasts. Here we used the fast-fixed point algorithm presented by Hyvärinen et al (Bingham and Hyvärinen, 2000). This algorithm transforms the observed data to the linear combination of source signals (or independent components) which are non-gaussian and mutually independent. The output of the ICA is a separating matrix, which is represented by two vectors defining a new basis of independent components. Results of the ICA on our MTR and T<sub>2</sub>\* data showed a fairly low inter-subject variability of the directions of the first vector (58±4°), which is assumed to represent myelin content. This low variability suggests stability of the decomposition process with respect to the spatial distribution of myelin-related source. Note that the current ICA framework is modular and the model would benefit from complementary sources of contrast sensitive to myelin content, such as T1 (Bock et al., 2009; Dinse et al., 2013; Sereno, 1991), T1w/T2w (Glasser and Van Essen, 2011), phase images (He and Yablonskiy, 2009) and diffusion data. While adding more metrics will likely increase the sensitivity and specificity to myelin, it is important to keep in mind that some metrics can share variance due to a shared MR contrast mechanism and/or artifactual contribution. For example, MTR contrast is partly driven by T1. In this study we chose to acquire T2\* and MTR. The rationale behind acquiring these two contrasts was to show a proof-of-concept for combining two myelin mapping techniques with very different

biophysical properties: susceptibility-related effect for T2\* and macromolecular-related magnetization transfer effect for MTR.

### Interpretations of the combined myelin estimation (CME) maps

The CME exhibited high values (>70%) in the primary motor cortex (BA4), in the primary somatosensory cortex (BA1, BA2 and BA3), in the visual cortex (BA17 & BA18) and in the auditory cortex (BA42). Contrariwise, the insula, the frontal and prefrontal cortex (BA8, BA9 & BA10) and the anterior cingulate cortex (BA24 & BA32) have low CME values (<30%). Seen as an indicator of myelin content, this pattern of CME across the cortex is in concordance with previous cortical myelin-oriented studies (Annese et al., 2004; Glasser and Van Essen, 2011; Glasser et al., 2014; Laule et al., 2008; Nieuwenhuys, 2013; Vogt, 1911). Moreover, the intra-regional standard deviation of the CME is low in comparison to that across the whole cortex. This suggests a fairly homogenous myelin estimate inside the putative cortical areas. This observation is consistent with previous studies showing homogeneous myeloarchitecture within functionally-defined areas. (Abdollahi et al., 2014; Bock et al., 2009; Geyer and Turner, 2013; Glasser and Van Essen, 2011; Glasser et al., 2014; Nieuwenhuys, 2013; Sereno, 1991).

The CME map was compared with existing myelin-related maps from the literature. The MR longitudinal relaxation time T1 has been shown to be closely related to myelin content in vivo (Dick et al., 2012; Koenig et al., 1990; Sigalovsky et al., 2006) and ex vivo (Mottershead et al., 2003; Schmierer et al., 2008, 2004) showing for example high correlation ( $r = 0.89$ ) between T1 relaxation time and myelin content in fixed brain (Schmierer et al., 2008). Recently, (Sereno et al., 2013) have computed high resolution quantitative R1 (inverse of T1) maps from PDw and T1w images according to the formalism developed by Helms et al. (2008) and including a correction for imperfect RF spoiling (Preibisch and Deichmann, 2009) in order to obtain an accurate estimation of the cortical myelin content. Moreover, the ratio between T1w and T2w images has been shown to be an accurate estimate of the relative myelin content across cortex (Glasser and Van Essen, 2011; Glasser et al., 2014). Glasser et al. (2014) have demonstrated that T1w/T2w maps reveals an observer-independent map of the area boundaries for dozens of cortical areas in a population-average analysis. Figure 11 shows a side-by-side comparison between our CME maps and the cortical myelin estimations based on T1w/T2w from Glasser et al. (Glasser and Van Essen, 2011; Glasser et al., 2014) and R1 (inverse of T1) contrast from Sereno et al. (Sereno et al., 2013). Strong similarities are observed across maps, notably high myelin indices in the motor, visual and auditory cortices and low myelin indices in the anterior frontal cortex and in the temporal cortex. Small details are also shared by all contrasts, for example the middle-high spot located in the frontal lobe of the left hemisphere (green circle), the middle-high spot in the superior temporal cortex of the right hemisphere (green circle) and the bright spot in the lateral occipital cortex (near BA19). More interestingly, some discrepancies are observed for the CME map (red circles), i.e. regions of strong contrast previously not seen in other metrics. For example, we can observe a stronger signal in CME maps than in R1 or T1w/T2w maps in the pars triangularis area (dashed-red circle, near BA47) and in the superior parietal area (red circle, near BA7). Further work is needed to validate these findings with histology.

We chose to analyse our data with respect to cortical parcellation offered by the PALS-B12 atlas, which aims at representing homogeneous cytoarchitecture within the human cortex as proposed by Brodmann (Brodmann, 1909). Borders of these regions are defined by the variation of the cells organization and structure of the cortex and are thought to represent functional units (Barbier et al., 2002; Jacot-Descombes et al., 2012; Lanzilotto et al., 2013). In analogy to the present study, we observe that regions representing specific functions of the human body (primary motor, auditory, visual) overlap with regions where CME was high. However, there is not necessarily a direct correspondence between myelo- and cyto-architecture (Geyer et al., 2011). Other atlases are available in the literature, notably the myeloarchitectonic atlas of Nieuwenhuys et al. (Nieuwenhuys et al. 2014), which divides the cortex into 180 myeloarchitectonic areas. A qualitative side-by-side comparison revealed some similarities between this atlas and the CME map. For example, in the pars triangularis region the bright spot visible in CME map only (dashed-red circle in Figure 11C) seems to overlap with area 57–58 in the Nieuwenhuys atlas (red circle in Supplementary material S3). We notice that this bright spot is in accordance with a previous ex vivo monkey histology (Cruz-Rizzolo et al., 2011). Moreover, the motor cortex in the CME map exhibits a multiple-line pattern along the central sulcus, which is also visible in the Nieuwenhuys atlas. Moreover, the motor cortex in the CME map exhibits a multiple-line pattern along the central sulcus, which is also visible in the Nieuwenhuys atlas.

It should be noted that CME is currently not calibrated on true myelin values. CME's limits (0% to 100%) were defined based on regions with qualitatively low and high myelin content (Annese et al., 2004; Glasser and Van Essen, 2011; Glasser et al., 2014; Laule et al., 2008; Nieuwenhuys, 2013; Vogt, 1911). Such a calibration procedure is challenging because ex vivo measures of myelin content may not be accurate for in vivo assessment. Histology and immunohistochemistry techniques may suffer from non-uniformity (Cruz-Rizzolo et al., 2011; Culling, 2013). Moreover, optical density measurements of the stain do not provide an accurate measure of myelin density because it does not probe the quantity of myelin in a slice (Culling, 2013). (Stüber et al., 2014) introduced the PIXE technique recently using complex experimental setup. Furthermore, MR parameters change post mortem due to fixation. For instance, the correlation of MTR with myelin content is much stronger before fixation (Schmierer et al., 2008). Moreover, image registration is not easy in such studies, and spatial sampling is limited. Finally, more knowledge is required about the relationship between CME and true myelin content. For example, here we assumed linearity, but this has to be verified before calibration procedure.

Concerning the fiber orientation dependency, we are aware that various models have been proposed in the literature. For example, (Bender and Klose, 2010; Denk et al., 2011) have shown that the fiber orientation dependence can be well described using the term  $\sin(\theta)^2$ . We have therefore compared our model with the  $\sin(\theta)^2$  model. Results were similar, with a square difference (averaged across all vertices) of 0.32 %<sup>2</sup> for ME\_MTR and 0.11 %<sup>2</sup> for ME\_T2\*.

The correlations with histological work of Braitenberg (Braitenberg, 1962) suggest that CME is a more specific marker for cortical myelin content compared to ME\_MTR or ME\_T2\* taken separately. We have also shown that ME\_MTR and ME\_T2\* are more

specific markers of myelin than MTR and T2\* (see Figure 8). This type of comparison is however limited by several factors. Firstly, the Braitenberg dataset was only limited to a few regions. Secondly, the study of Braitenberg was hampered by imperfect tissue fixation and staining, which added potential biases in the measures.

### Limitations and futures studies

T<sub>2</sub>\* volumes were acquired with anisotropic voxels in order to maintain a high in-plane resolution (0.3×0.3 mm). Anisotropic voxels are subject to more inhomogeneous partial volume effect during the cortical sampling. In the future, EPI-Based multi-echo measurements (Zwanenburg et al., 2011) may sufficiently accelerate acquisition to allow use of isotropic voxels. MTR volumes were acquired with isotropic voxels, despite a somewhat low resolution (1.2mm) in comparison with the thickness of the cortex. Future studies could benefit from MT-prepared multi-echo EPI (Helms and Hagberg, 2005) in order to acquire faster MT-weighted images and potentially increase the spatial resolution thanks to the higher SNR efficiency of EPI sequences. However it is important to keep in mind that EPI measurement suffers from geometric distortions, which are difficult to perfectly correct using standard approaches (fieldmap-based or non-rigid alignment). Residual distortions would lead to imperfect registration to the cortical surface and hence lead to potentially wrong values when sampling along the cortical ribbon.

The MMEM used a normalization procedure based on regions that are known to be highly and poorly myelinated. Thus, the output of the MMEM does not give an absolute measure of myelin content, but rather an indicator of relative level of myelin compared to other brain areas. Furthermore, it could be argued the choice of regions for normalization purpose was not adequate, however the robustness of the resulting MMEM coefficients was fairly high. For example, when using only BA4 (high myelin) and BA9 (low myelin), the resulting coefficients were less than 1% different compared to the results presented in this study.

Validation is essential to these types of MRI studies. Although CME maps showed remarkably high spatial correspondence with previous *in vivo* and postmortem studies (Annese et al., 2004; Glasser and Van Essen, 2011; Glasser et al., 2014; Laule et al., 2008; Nieuwenhuys, 2013; Vogt, 1911) it remains essential to further compare MRI maps with full cortex histology samples stained for myelin. However, limitations exist with histological staining, as it does not necessarily represent quantitative measure of myelin content and is hampered by the attachment properties of the tissue (depends on preparation, fixation, etc.) (Jain et al., 1998; Pistorio et al., 2006).

The multivariate myelin estimation model has the potential to be useful in assessing early cortical changes in myelin in patients with neurodegenerative diseases such as multiple sclerosis.

### Supplementary Material

Refer to Web version on PubMed Central for supplementary material.

## Acknowledgments

We thank Benjamin De Leener, Tanguy Duval, Simon Lévy, Blanche Perraud, Nikola Stikov and Yves Goussard (Polytechnique Montreal), Pierre Bellec (Université de Montréal), Céline Louapre and Costanza Gianni (A. A. Martinos Center, Boston), Gaëlle Seret (Polytechnique Paris) and Jérémie Pilon (Danone Research) for helpful discussions. This work was supported by the National Multiple Sclerosis Society [FG 1892A1/1, 4281-RG-A-1], by the National Center for Research Resources [P41-RR14075], the Fonds de Recherche du Québec – Santé (FRQS), the Fonds de Recherche du Québec – Nature et Technologies (2015-PR-182754), the Quebec BioImaging Network (QBIN), the Natural Sciences and Engineering Research Council of Canada (NSERC) and the Polytechnique MEDITIS program.

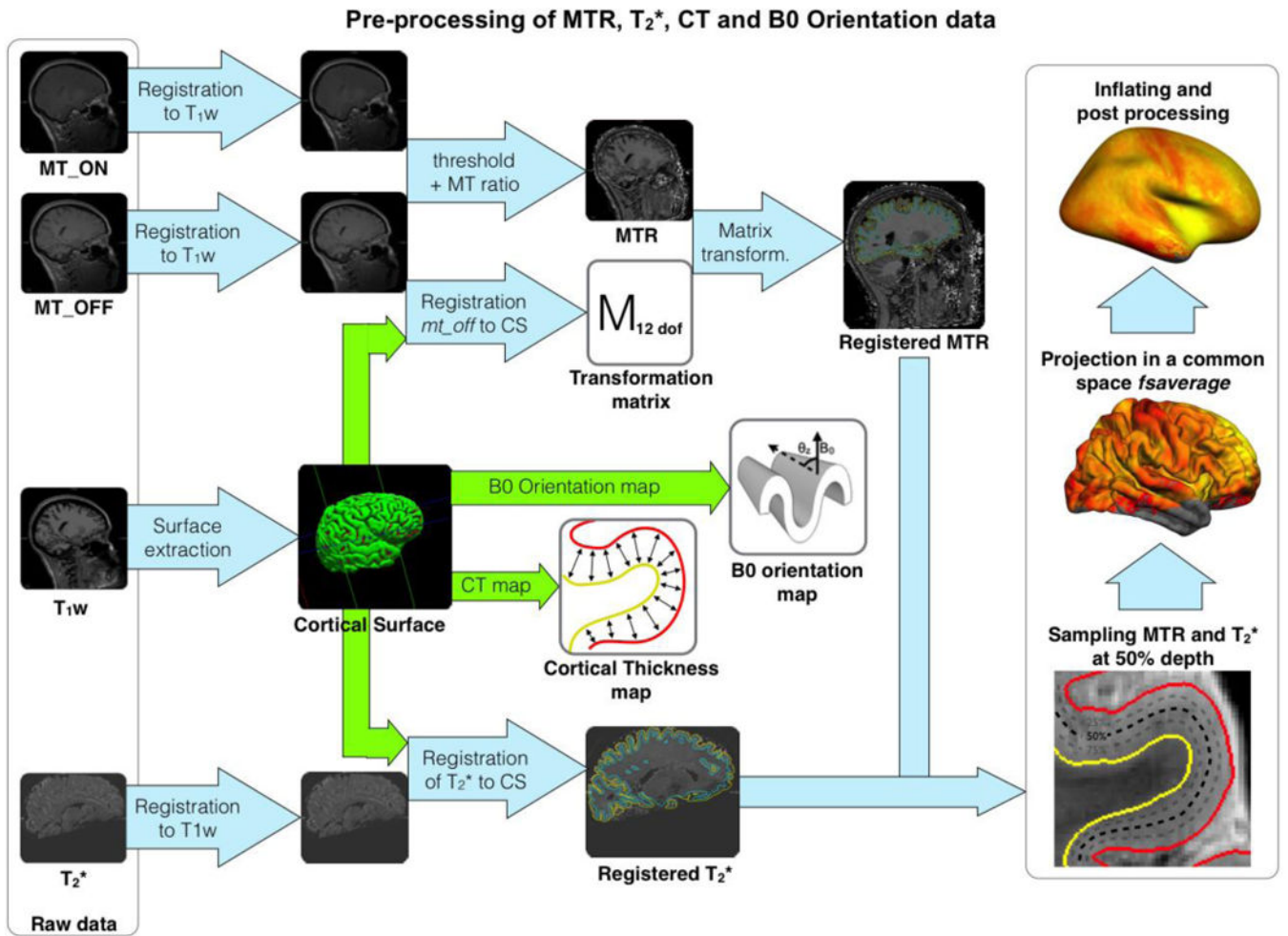
## References

- Abdollahi RO, Kolster H, Glasser MF, Robinson EC, Coalson TS, Dierker D, Jenkinson M, Van Essen DC, Orban GA. Correspondences between retinotopic areas and myelin maps in human visual cortex. *Neuroimage*. 2014; 99:509–524. [PubMed: 24971513]
- Annese J, Pitiot A, Dinov ID, Toga AW. A myelo-architectonic method for the structural classification of cortical areas. *Neuroimage*. 2004; 21:15–26. [PubMed: 14741638]
- Barbier EL, Marrett S, Danek A, Vortmeyer A, van Gelderen P, Duyn J, Bandettini P, Grafman J, Koretsky AP. Imaging cortical anatomy by high-resolution MR at 3.0T: detection of the stripe of Gennari in visual area 17. *Magn Reson Med*. 2002; 48:735–738. [PubMed: 12353293]
- Bender B, Klose U. The in vivo influence of white matter fiber orientation towards B0 on T2\* in the human brain. *NMR Biomed*. 2010; 23:1071–1076. [PubMed: 20665897]
- Berry I, Barker GJ, Barkhof F, Campi A, Dousset V, Franconi JM, Gass A, Schreiber W, Miller DH, Tofts PS. A multicenter measurement of magnetization transfer ratio in normal white matter. *J Magn Reson Imaging*. 1999; 9:441–446. [PubMed: 10194715]
- Bingham E, Hyvärinen A. A fast fixed-point algorithm for independent component analysis of complex valued signals. *Int J Neural Syst*. 2000; 10:1–8. [PubMed: 10798706]
- Bock NA, Kocharyan A, Liu JV, Silva AC. Visualizing the entire cortical myelination pattern in marmosets with magnetic resonance imaging. *J Neurosci Methods*. 2009; 185:15–22. [PubMed: 19737577]
- Braitenberg V. A note on myeloarchitectonics. *J Comp Neurol*. 1962; 118:141–156. [PubMed: 13872421]
- Brodmann, K. BRODMANN'S Localisation in the Cerebral Cortex. Springer; 1909.
- Chen JTH, Easley K, Schneider C, Nakamura K, Kidd GJ, Chang A, Staugaitis SM, Fox RJ, Fisher E, Arnold DL, Trapp BD. Clinically feasible MTR is sensitive to cortical demyelination in MS. *Neurology*. 2013; 80:246–252. [PubMed: 23269598]
- Clarkson MJ, Cardoso MJ, Ridgway GR, Modat M, Leung KK, Rohrer JD, Fox NC, Ourselin S. A comparison of voxel and surface based cortical thickness estimation methods. *Neuroimage*. 2011; 57:856–865. [PubMed: 21640841]
- Cohen-Adad J. What can we learn from T2\* maps of the cortex? *Neuroimage*. 2014; 93(Pt 2):189–200. [PubMed: 23357070]
- Cohen-Adad J, Benner T, Greve D, Kinkel RP, Radding A, Fischl B, Rosen BR, Mainero C. In vivo evidence of disseminated subpial T2\* signal changes in multiple sclerosis at 7 T: a surface-based analysis. *Neuroimage*. 2011; 57:55–62. [PubMed: 21511042]
- Cohen-Adad J, Polimeni JR, Helmer KG, Benner T, McNab JA, Wald LL, Rosen BR, Mainero C. T2\* mapping and B0 orientation-dependence at 7 T reveal cyto- and myeloarchitecture organization of the human cortex. *Neuroimage*. 2012; 60:1006–1014. [PubMed: 22270354]
- Cruz-Rizzolo RJ, De Lima MAX, Ervolino E, de Oliveira JA, Casatti CA. Cyto-, myelo- and chemoarchitecture of the prefrontal cortex of the Cebus monkey. *BMC Neurosci*. 2011; 12:6. [PubMed: 21232115]
- Culling, CFA. *Handbook of Histopathological and Histochemical Techniques Including Museum Techniques*. 3rd. Burlington Elsevier; 2013.
- Dale AM, Fischl B, Sereno MI. I. Segmentation and Surface Reconstruction. *Neuroimage*. 1999; 9:179–194. [PubMed: 9931268]

- Deistung A, Schäfer A, Schweser F, Biedermann U, Turner R, Reichenbach JR. Toward in vivo histology: a comparison of quantitative susceptibility mapping (QSM) with magnitude-, phase-, and  $R2^*$ -imaging at ultra-high magnetic field strength. *Neuroimage*. 2013; 65:299–314. [PubMed: 23036448]
- Denk C, Hernandez Torres E, MacKay A, Rauscher A. The influence of white matter fibre orientation on MR signal phase and decay. *NMR Biomed*. 2011; 24:246–252. [PubMed: 21404336]
- Derakhshan M, Caramanos Z, Narayanan S, Arnold DL, Louis Collins D. Surface-based analysis reveals regions of reduced cortical magnetization transfer ratio in patients with multiple sclerosis: a proposed method for imaging subpial demyelination. *Hum Brain Mapp*. 2014; 35:3402–3413. [PubMed: 24356893]
- Dick F, Tierney AT, Lutti A, Josephs O, Sereno MI, Weiskopf N. In vivo functional and myeloarchitectonic mapping of human primary auditory areas. *J Neurosci*. 2012; 32:16095–16105. [PubMed: 23152594]
- Dinse, J.; Waehnert, M.; Tardif, CL.; Schäfer, A.; Geyer, S.; Turner, R.; Bazin, PL. A Histology-Based Model of Quantitative T1 Contrast for In-vivo Cortical Parcellation of High-Resolution 7 Tesla Brain MR Images. Springer. , editor. *Medical Image Computing and Computer-Assisted Intervention*; 2013. p. 51-58.2013
- Duyn JH, van Gelderen P, Li TQ, de Zwart JA, Koretsky AP, Fukunaga M. High-field MRI of brain cortical substructure based on signal phase. *Proc Natl Acad Sci U S A*. 2007; 104:11796–11801. [PubMed: 17586684]
- Fischl B. *FreeSurfer*. *Neuroimage*. 2012; 62:774–781. [PubMed: 22248573]
- Fischl B, Sereno MI, Dale AM. II: Inflation, Flattening, and a Surface-Based Coordinate System. *Neuroimage*. 1999; 9:195–207. [PubMed: 9931269]
- Flechsig, PE. *Anatomie des menschlichen Gehirns und Rückenmarks auf myelogenetischer Grundlage*. Thieme; 1920.
- Fukunaga M, Li TQ, van Gelderen P, de Zwart JA, Shmueli K, Yao B, Lee J, Maric D, Aronova MA, Zhang G, Leapman RD, Schenck JF, Merkle H, Duyn JH. Layer-specific variation of iron content in cerebral cortex as a source of MRI contrast. *Proc Natl Acad Sci U S A*. 2010; 107:3834–3839. [PubMed: 20133720]
- Geyer, S.; Turner, R. *Microstructural parcellation of the human cerebral cortex from Brodmann’s post-mortem map to in vivo mapping with high-field magnetic resonance imaging* Berlin. New York: Springer; 2013. c2013
- Geyer S, Weiss M, Reimann K, Lohmann G, Turner R. Microstructural Parcellation of the Human Cerebral Cortex – From Brodmann’s Post-Mortem Map to in vivo Mapping with High-Field Magnetic Resonance Imaging. *Front Hum Neurosci*. 2011; 5:19. [PubMed: 21373360]
- Glasser MF, Goyal MS, Preuss TM, Raichle ME, Van Essen DC. Trends and properties of human cerebral cortex: correlations with cortical myelin content. *Neuroimage*. 2014; 93(Pt 2):165–175. [PubMed: 23567887]
- Glasser MF, Van Essen DC. Mapping human cortical areas in vivo based on myelin content as revealed by T1- and T2-weighted MRI. *J Neurosci*. 2011; 31:11597–11616. [PubMed: 21832190]
- Govindarajan ST, Cohen-Adad J, Sormani MP, Fan AP, Louapre C, Mainero C. Reproducibility of  $T2^*$  mapping in the human cerebral cortex in vivo at 7 Tesla MRI. *J Magn Reson Imaging*. 2014
- Greve DN, Fischl B. Accurate and robust brain image alignment using boundary-based registration. *Neuroimage*. 2009; 48:63–72. [PubMed: 19573611]
- He X, Yablonskiy DA. Biophysical mechanisms of phase contrast in gradient echo MRI. *Proc Natl Acad Sci U S A*. 2009; 106:13558–13563. [PubMed: 19628691]
- Helms G, Dathe H, Dechent P. Quantitative FLASH MRI at 3T using a rational approximation of the Ernst equation. *Magn Reson Med*. 2008; 59:667–672. [PubMed: 18306368]
- Helms G, Hagberg GE. Quantification of magnetization transfer and relaxation rates by MT- prepared multi-echo EPI. *Proc Intl Soc Mag Reson Med*. 2005; 13:2221.
- Henkelman RM, Stanisz GJ, Graham SJ. Magnetization transfer in MRI: a review. *NMR Biomed*. 2001; 14:57–64. [PubMed: 11320533]
- Hernando D, Vigen KK, Shimakawa A, Reeder SB.  $R2^*$  mapping in the presence of macroscopic  $B0$  field variations. *Magn Reson Med*. 2012; 68:830–840. [PubMed: 22161866]

- Hwang D, Kim DH, Du YP. In vivo multi-slice mapping of myelin water content using T2\* decay. *Neuroimage*. 2010; 52:198–204. [PubMed: 20398770]
- Hyvärinen A, Oja E. Independent component analysis: algorithms and applications. *Neural Netw*. 2000; 13:411–430. [PubMed: 10946390]
- Jacot-Descombes S, Uppal N, Wicinski B, Santos M, Schmeidler J, Giannakopoulos P, Heinsen H, Heinsen H, Schmitz C, Hof PR. Decreased pyramidal neuron size in Brodmann areas 44 and 45 in patients with autism. *Acta Neuropathol*. 2012; 124:67–79. [PubMed: 22467063]
- Jain N, Catania K, Kaas J. A histologically visible representation of the fingers and palm in primate area 3b and its immutability following long-term deafferentations. *Cereb Cortex*. 1998; 8(3):227–36. [PubMed: 9617917]
- Kim, M.; Cercignani, M. Chapter 3.4 – Magnetization Transfer. In: Wheeler-Kingshott, JC-AAM., editor. *Quantitative MRI of the Spinal Cord*. Academic Press; San Diego: 2014. p. 164-180.
- Koenig SH, Brown RD 3rd, Spiller M, Lundbom N. Relaxometry of brain: why white matter appears bright in MRI. *Magn Reson Med*. 1990; 14:482–495. [PubMed: 2355830]
- Lanzilotto M, Perciavalle V, Lucchetti C. Auditory and visual systems organization in Brodmann Area 8 for gaze-shift control: where we do not see, we can hear. *Front Behav Neurosci*. 2013; 7:198. [PubMed: 24339805]
- Laule C, Kozlowski P, Leung E, Li DKB, Mackay AL, Moore GRW. Myelin water imaging of multiple sclerosis at 7 T: correlations with histopathology. *Neuroimage*. 2008; 40:1575–1580. [PubMed: 18321730]
- Lee J, Shmueli K, Kang BT, Yao B, Fukunaga M, van Gelderen P, Palumbo S, Bosetti F, Silva AC, Duyn JH. The contribution of myelin to magnetic susceptibility-weighted contrasts in high-field MRI of the brain. *Neuroimage*. 2012; 59:3967–3975. [PubMed: 22056461]
- Lee J, van Gelderen P, Kuo LW, Merkle H, Silva AC, Duyn JH. T2\*-based fiber orientation mapping. *Neuroimage*. 2011; 57:225–234. [PubMed: 21549203]
- Levesque IR, Pike GB. Characterizing healthy and diseased white matter using quantitative magnetization transfer and multicomponent T2 relaxometry: A unified view via a four-pool model. *Magn Reson Med*. 2009; 62:1487–1496. [PubMed: 19859946]
- Li D, Wang Y, Waight DJ. Blood oxygen saturation assessment in vivo using T2\* estimation. *Magn Reson Med*. 1998; 39:685–690. [PubMed: 9581597]
- Li TQ, van Gelderen P, Merkle H, Talagala L, Koretsky AP, Duyn J. Extensive heterogeneity in white matter intensity in high-resolution T2\*-weighted MRI of the human brain at 7.0 T. *Neuroimage*. 2006; 32:1032–1040. [PubMed: 16854600]
- Li TQ, Yao B, van Gelderen P, Merkle H, Dodd S, Talagala L, Koretsky AP, Duyn J. Characterization of T2\* heterogeneity in human brain white matter. *Magn Reson Med*. 2009; 62:1652–1657. [PubMed: 19859939]
- Mainero C, Louapre C, Govindarajan ST, Gianni C, Nielsen AS, Cohen-Adad J, Sloane J, Kinkel RP. A gradient in cortical pathology in multiple sclerosis by in vivo quantitative 7 T imaging. *Brain*. 2015; 138:932–945. [PubMed: 25681411]
- Mottershead JP, Schmierer K, Clemence M, Thornton JS, Scaravilli F, Barker GJ, Tofts PS, Newcombe J, Cuzner ML, Ordidge RJ, McDonald WI, Miller DH. High field MRI correlates of myelin content and axonal density in multiple sclerosis. *J Neurol*. 2003; 250:1293–1301. [PubMed: 14648144]
- Nieuwenhuys R. The myeloarchitectonic studies on the human cerebral cortex of the Vogt-Vogt school, and their significance for the interpretation of functional neuroimaging data. *Brain Struct Funct*. 2013; 218:303–352. [PubMed: 23076375]
- Pike Bruce G. Pulsed Magnetization Transfer Contrast in Gradient Echo Imaging: Two-Pool Analytic Description of Signal Response. *Magn Reson Med*. 1996; 36:95–103. [PubMed: 8795027]
- Pistorio AL, Hendry SH, Wang X. A modified technique for high-resolution staining of myelin. *J Neurosci Methods*. 2006; 153:135–146. [PubMed: 16310256]
- Pitt D, Boster A, Pei W, Bs EW, Bs AJ, Zachariah BS, C R, Rammohan K, Knopp MV, Schmalbrock P. Imaging Cortical Lesions in Multiple Sclerosis With Ultra-High-Field Magnetic Resonance Imaging. *Arch Neurol*. 2010:812–818. [PubMed: 20625086]

- Postelnicu G, Zollei L, Fischl B. Combined volumetric and surface registration. *IEEE Trans Med Imaging*. 2009; 28:508–522. [PubMed: 19273000]
- Preibisch C, Deichmann R. Influence of RF spoiling on the stability and accuracy of T1 mapping based on spoiled FLASH with varying flip angles. *Magn Reson Med*. 2009; 61:125–135. [PubMed: 19097220]
- Reuter M, Rosas HD, Fischl B. Highly accurate inverse consistent registration: a robust approach. *Neuroimage*. 2010; 53:1181–1196. [PubMed: 20637289]
- Sati P, Silva AC, van Gelderen P, Gaitan MI, Wohler JE, Jacobson S, Duyn JH, Reich DS. In vivo quantification of T2\* anisotropy in white matter fibers in marmoset monkeys. *Neuroimage*. 2012; 59:979–985. [PubMed: 21906687]
- Schmierer K, Scaravilli F, Altmann DR, Barker GJ, Miller DH. Magnetization transfer ratio and myelin in postmortem multiple sclerosis brain. *Ann Neurol*. 2004; 56:407–415. [PubMed: 15349868]
- Schmierer K, Wheeler-Kingshott CAM, Tozer DJ, Boulby PA, Parkes HG, Yousry TA, Scaravilli F, Barker GJ, Tofts PS, Miller DH. Quantitative magnetic resonance of postmortem multiple sclerosis brain before and after fixation. *Magn Reson Med*. 2008; 59:268–277. [PubMed: 18228601]
- Sereno MI. Language And The Primate Brain. *Proceedings Thirteenth Annual Conference of the Cognitive Science Society*. 1991
- Sereno MI, Lutti A, Weiskopf N, Dick F. Mapping the human cortical surface by combining quantitative T(1) with retinotopy. *Cereb Cortex*. 2013; 23:2261–2268. [PubMed: 22826609]
- Sigalovsky IS, Fischl B, Melcher JR. Mapping an intrinsic MR property of gray matter in auditory cortex of living humans: a possible marker for primary cortex and hemispheric differences. *Neuroimage*. 2006; 32:1524–1537. [PubMed: 16806989]
- Spees WM, Yablonskiy DA, Oswood MC, Ackerman JJH. Water Proton MR Properties of Human Blood at 1.5 Tesla: Magnetic Susceptibility, T1, T2, T\*2, and Non-Lorentzian Signal Behavior. *Magn Reson Med*. 2001; 45:533–542. [PubMed: 11283978]
- Stüber C, Morawski M, Schäfer A, Labadie C, Wähnert M, Leuze C, Streicher M, Barapatre N, Reimann K, Geyer S, Spemann D, Turner R. Myelin and iron concentration in the human brain: a quantitative study of MRI contrast. *Neuroimage*. 2014; 93(Pt 1):95–106. [PubMed: 24607447]
- Tardif CL, Bedell BJ, Eskildsen SF, Collins DL, Pike GB. Quantitative magnetic resonance imaging of cortical multiple sclerosis pathology. *Mult Scler Int*. 2012; 2012:742018. [PubMed: 23213531]
- Van der Kouwe AJW, Benner T, Salat DH, Fischl B. Brain morphometry with multiecho MPRAGE. *Neuroimage*. 2008; 40:559–569. [PubMed: 18242102]
- Van Essen DC. A Population-Average, Landmark- and Surface-based (PALS) atlas of human cerebral cortex. *Neuroimage*. 2005; 28:635–662. [PubMed: 16172003]
- Vogt O. Die Myeloarchitektonik des Isocortex parietalis. *Journal für Psychologie und Neurologie*. 1911; 18:379–390.
- Xie L, Wu J. Global optimal ICA and its application in MEG data analysis. *Neurocomputing*. 2006; 69:2438–2442.
- Zwanenburg JJM, Versluis MJ, Luijten PR, Petridou N. Fast high resolution whole brain T2\* weighted imaging using echo planar imaging at 7T. *Neuroimage*. 2011; 56:1902–1907. [PubMed: 21440070]

**Figure 1.**

Pre-processing framework. The cortical surface was extracted with freesurfer from an anatomical  $T_1$ -weighted volume. MT data:  $mt_{on}$  and  $mt_{off}$  volumes were registered to the  $T_1$ -w volume (Reuter et al., 2010), then the MT ratio (MTR) was computed.  $mt_{off}$  was registered to the cortical surface (CS) using boundary based registration technique (12 d.o.f.) (Greve and Fischl, 2009). The transformation matrix of the registration was applied to the MTR volume.  $T_2^*$  volume was registered to the  $T_1$ -w volume using header information. Then,  $T_2^*$  volume was registered to the cortical surface using boundary based registration (9 d.o.f.). MTR and  $T_2^*$  cortical maps were computed at each vertex along the mid-cortical surface. Cortical thickness map was acquired by computing the distance between white and pial surfaces for each vertex.  $B_0$  orientation map was computed from the angle between the normal of the cortical surface and the orientation of the  $B_0$  field. Lastly, the four metrics ( $T_2^*$ , MTR, cortical thickness and  $B_0$  orientation) were projected to a common space (*fsaverage*) using a spherical averaging procedure (FreeSurfer).

## Multivariate myelin estimation model (MMEM) applied for each Subject

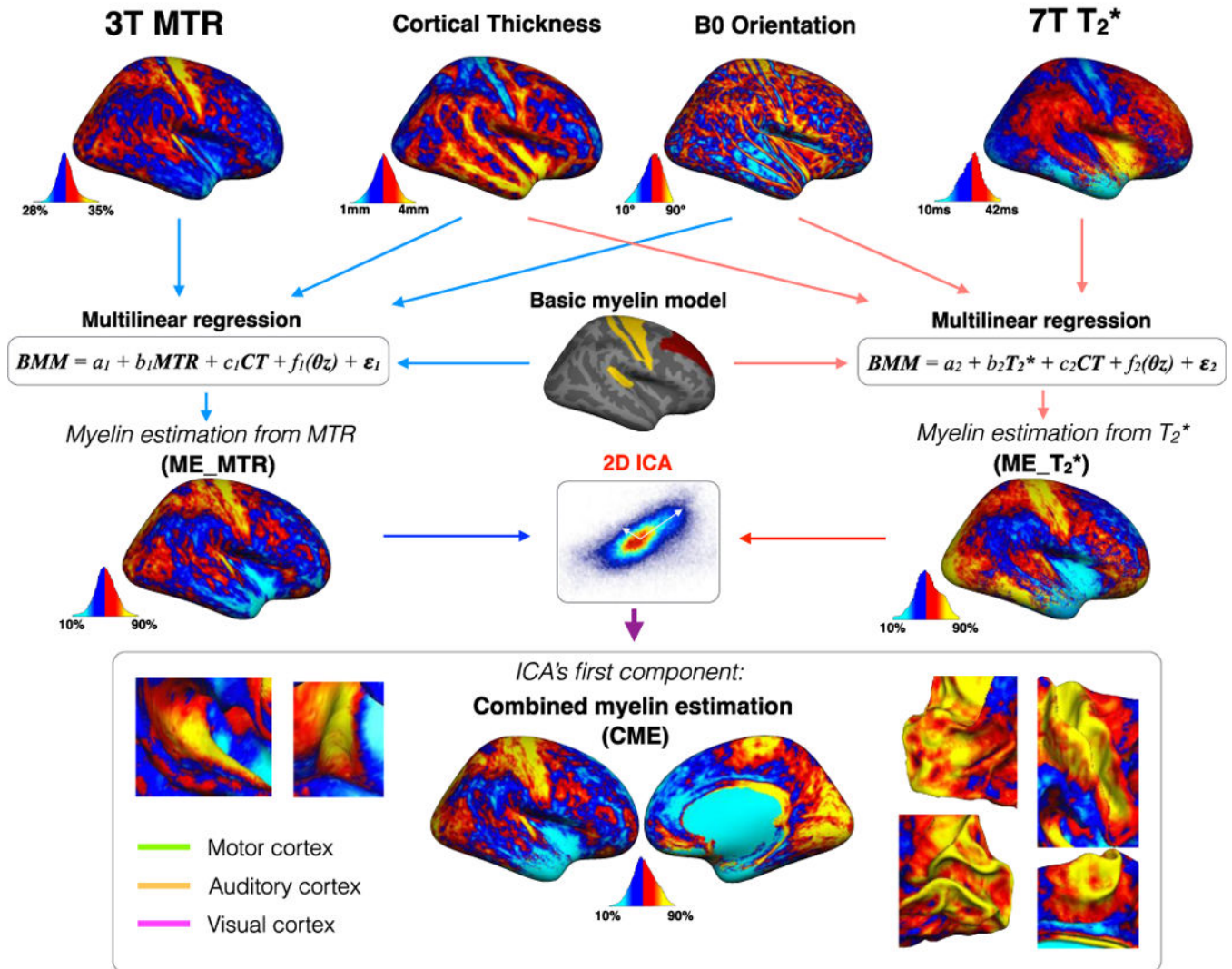


**Figure 2.**

Multivariate myelin estimation model (MMEM). MMEM aimed to estimate a cortical myelin map using MTR,  $T_2^*$ , cortical thickness (CT) and B0 orientation maps. The MMEM was divided into two steps. Firstly, two maps were estimated using multi-linear regressions: one using MTR, CT and B0 orientation (ME\_MTR) and one using  $T_2^*$ , CT and B0 orientation (ME\_T2\*). ME\_MTR and ME\_T2\* maps represent myelin-correlated values corrected for partial volume effect and fibers orientation. In order to merge MTR and  $T_2^*$  within the same framework, both linear regressions were performed with a common dependent variable (BMM). Secondly, the shared information between ME\_MTR and ME\_T2\* was extracted using ICA decomposition, for each subject. The ICA decomposed the signal into two component that are mathematically independent. The ‘so-called’ first component of the ICA was the source that share the highest variance between ME\_MTR and ME\_T2\*. The hypothesis being that the first component of the ICA was an indicator for myelin content.

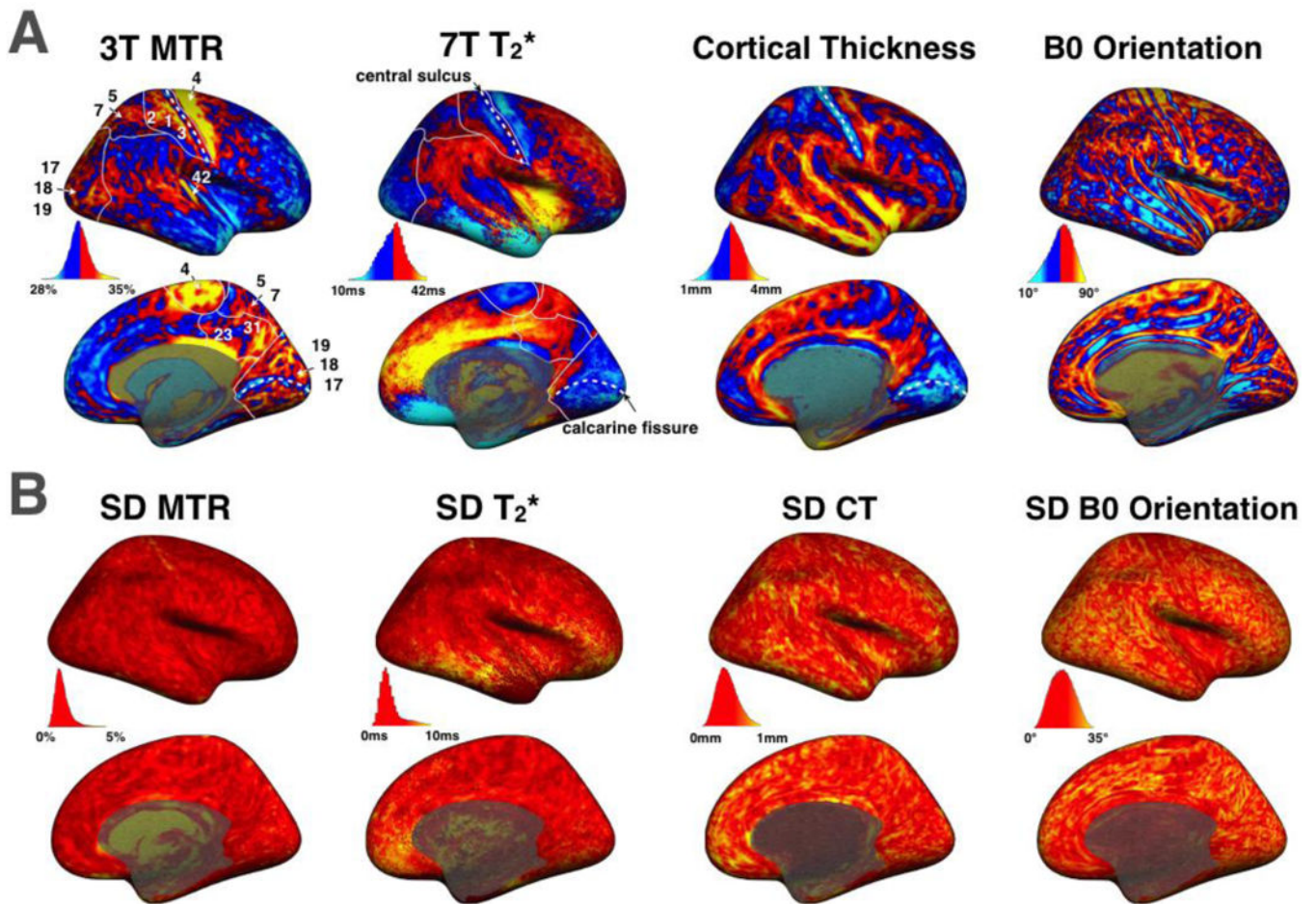


**Figure 3.**

(A) Maps averaged across subjects of MTR, T<sub>2</sub>\*, cortical thickness (CT) and B0 orientation. In MTR and T<sub>2</sub>\* maps, white lines are showing the borders of the primary somatosensory cortex (BA1, BA2 & BA3), the somatosensory association cortex (BA5 & BA7), the posterior cingulate cortex (BA31 & BA23) and the visual cortex (BA17, BA18 & BA19). Arrow are also showing the primary motor cortex (BA4) and the primary auditory cortex (BA42). White dashed lines are showing the central sulcus and the calcarine fissure. The colormap was thresholded (mid-value of each distribution) to enhance its dynamic. For unthresholded maps, see Supplementary Material S4. (B) Maps of the standard deviation across subjects for MTR, T<sub>2</sub>\*, CT and B0 orientation.

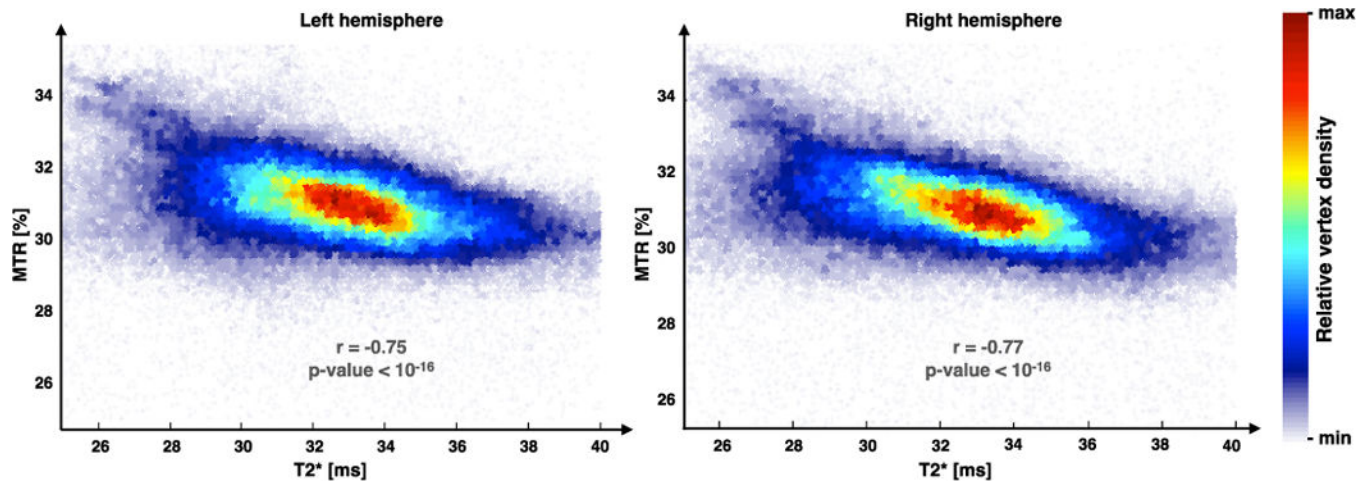


**Figure 4.**

Pearson's correlations between MTR and  $T_2^*$  maps averaged across subjects. Strong correlations were observed in right ( $r = -0.77$ ) and left ( $r = -0.75$ ) hemispheres. The colormap shows the data-point density in the scatter and suggest a 2D Gaussian tendency well defined in the center of the distribution.

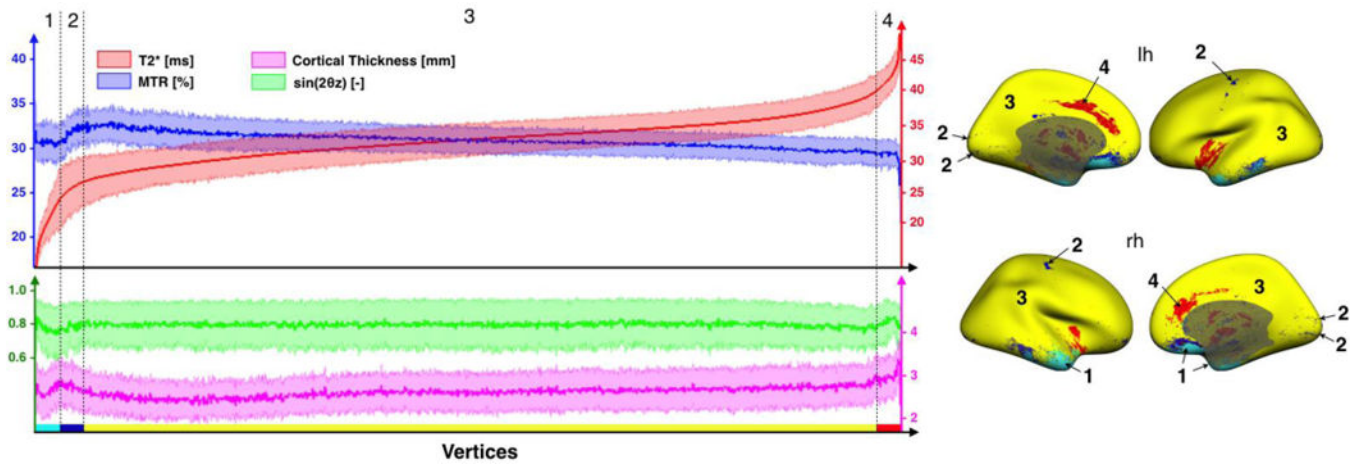


**Figure 5.**

The graph on the left panel shows the distribution of the four signals used in the MMEM: MTR (blue), T<sub>2</sub>\* (red), CT (magenta) and B<sub>0</sub> orientation (green). The abscissa represents vertices defining the cortical surface (total number of vertices = 163,842). For clarity, the vertices order was chosen to make T<sub>2</sub>\* increasing and values were smoothed along the abscissa (100-point window). Error strips represent the inter-subjects SD. Similar trends are observed between the left and the right hemispheres, therefore only the signal of the right hemisphere was plotted. The distribution graph was divided into four ensembles of vertices (1, 2, 3 & 4) based on their signal's shapes. Vertices corresponding to these regions are plotted on the right panel with the respective colors: light blue, dark blue, yellow & red.

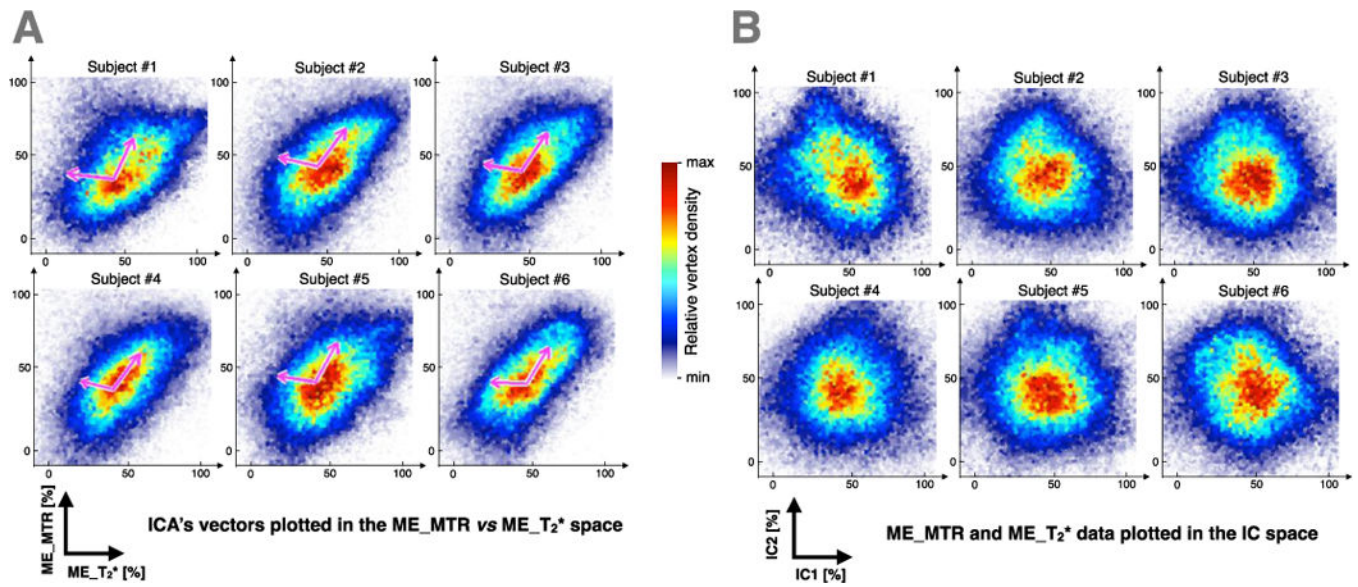


**Figure 6.**

(A) Scatters of the individual data (ME\_MTR vs ME\_T2\*) and both ICA's resulting components (pink arrows). For each subjects, first ICA's component is the one sharing most variance between ME\_MTR and ME\_T2\* (pointing upper right). (B) Projection of the ME\_MTR and ME\_T2\* data into the space defined by the two ICA's components. These graphs are used to assess the non-correlation ( $r < 0.06$ ) of the resulting set of data. The colormap shows the data-point density in the scatters.

Combined myelin estimation in the *in vivo* human cortex

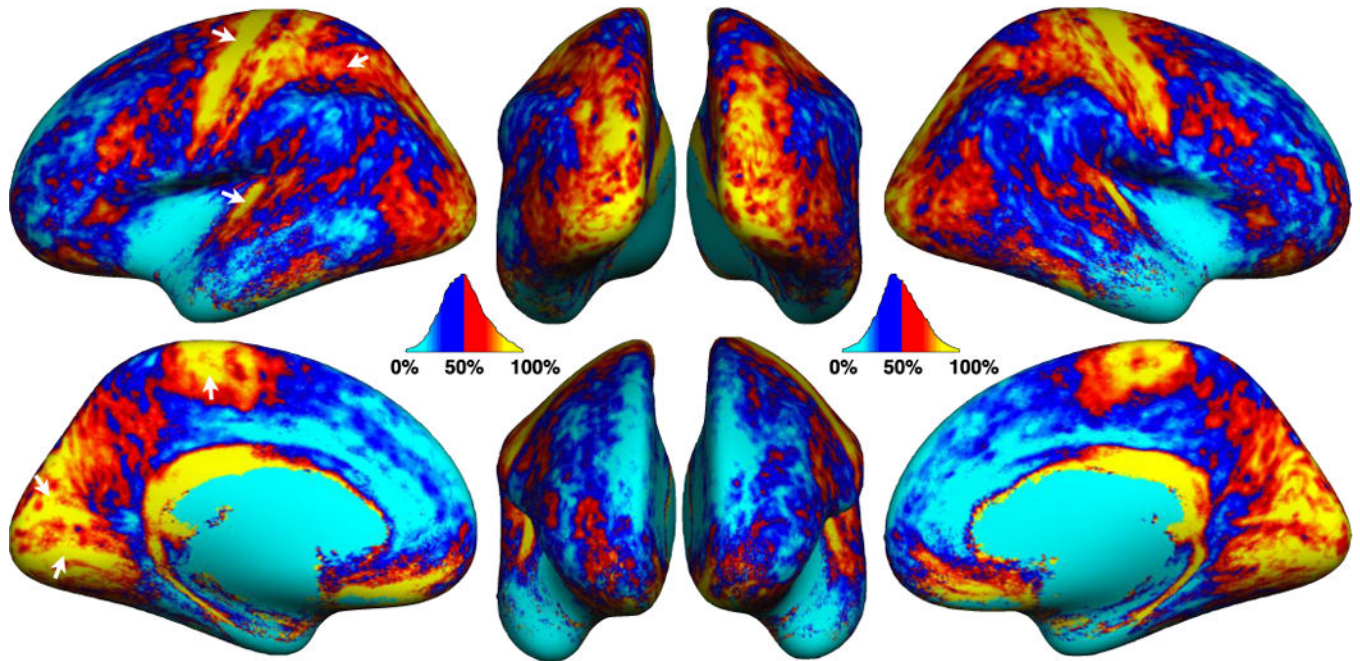


**Figure 7.**

Average map of the Combined Myelin Estimation (CME). The mean and SD of CME across the cortex was  $50.3 \pm 0.7$ . Overall, we notice a high myelin estimation (yellow/red) in the primary motor cortex  $BA4=74 \pm 3\%$  (here, % refers to the CME metric, and  $\pm 3\%$  refers to the SD across subjects) and in the primary somatosensory cortex ( $BA1=67 \pm 7\%$ ,  $BA2=59 \pm 4\%$  and  $BA3=63 \pm 13\%$ ). Moreover, a high myelin estimation is also observed in the visual cortex ( $BA17=67 \pm 5\%$  &  $BA18=68 \pm 6\%$ ) and the auditory cortex ( $BA42=57 \pm 10\%$ ).

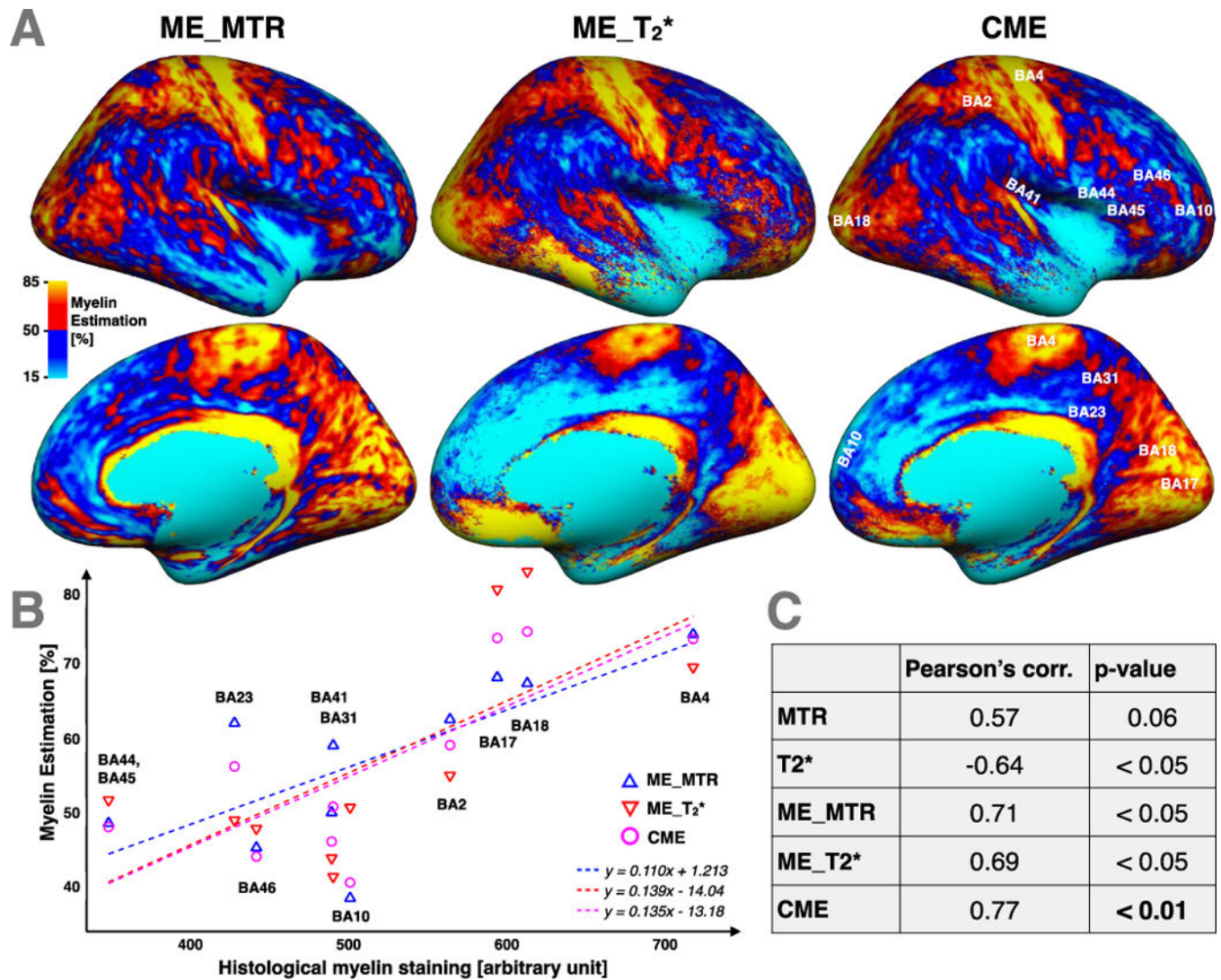


**Figure 8.**

(A) Side-by-side comparison between CME maps and its both parents contrasts: ME\_MTR and ME\_T2\*. Major differences between ME\_MTR and ME\_T2\* are circled by white circles. The CME map is labelled with the Brodmann areas used in the histological comparison. (B) Comparison between our myelin-related maps (CME, ME\_MTR and ME\_T2\*) and previous cortical myelin content histology data performed by Braitenberg (Braitenberg, 1962) in different Brodmann areas. The equations of the linear regressions are displayed at the bottom-right of the graph. The linear regression between T2\* and histological myelin staining (HMS) is:  $T2^* = -15.2 \cdot 10^{-3} [\text{ms/a.u.}] \cdot \text{HMS} + 39.4 [\text{ms}]$ ; and the linear regression between MTR and HMS is:  $\text{MTR} = 4.2 \cdot 10^{-3} [\%/\text{a.u.}] \cdot \text{HMS} + 29.0 [\%]$ . (C) Pearson's correlations coefficients between MTR vs Histology, T2\* vs Histology, ME\_MTR vs Histology, ME\_T2\* vs Histology and CME vs Histology and their respective P-values. Results suggests first that ME\_MTR and ME\_T2\* contrasts are relevant marker of the cortical myelin content and second that CME is a more specific marker for cortical myelin content than ME\_MTR or ME\_T2\* taken separately.

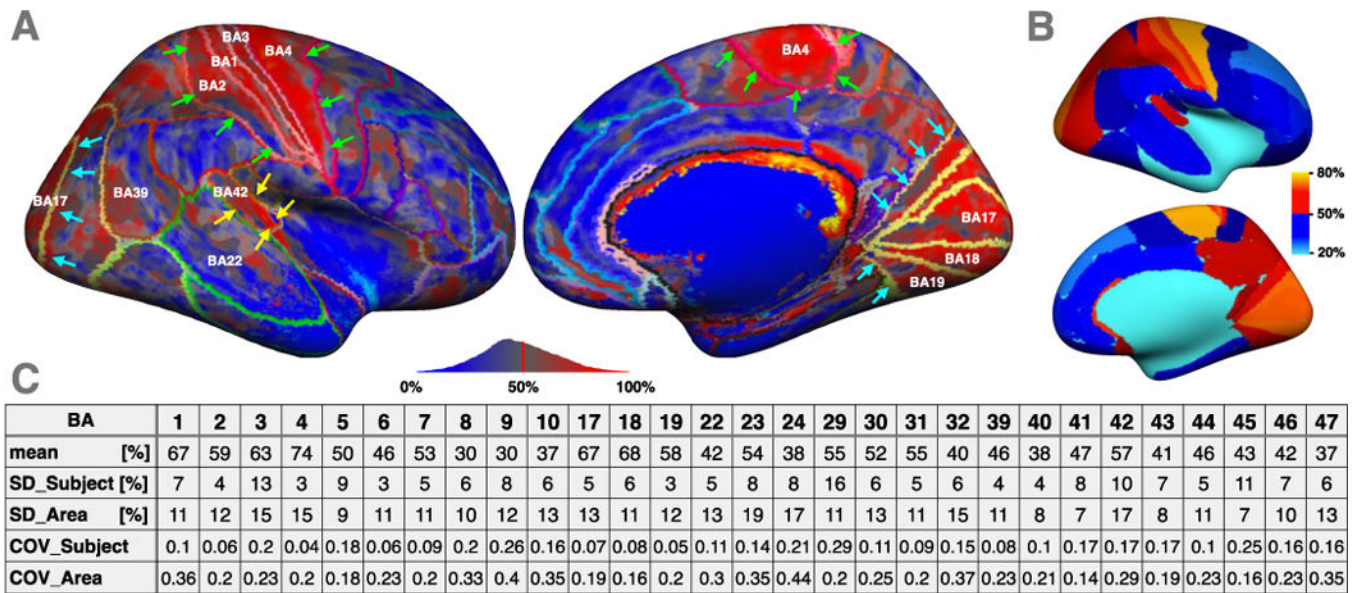


**Figure 9.** (A) CME map with an overlay of the PALS-B12 Brodmann Areas (BA). This figure shows a fair adequation between variations of CME and BA borders, for instance in BA1, BA2, BA3 and BA4 (primary motor and primary somatosensory cortex, green arrows), in BA17, BA18, BA19 (visual cortex, blue arrows) and in BA42 (auditory cortex, yellow arrow). (B) CME map averaged within each BA. (C) Mean BA values, as well as the inter-subject SD and the intra-area SD. In comparison with the SD across the entire cortex (26.5%), the intra-area SD is fairly low (in average 11.9%).

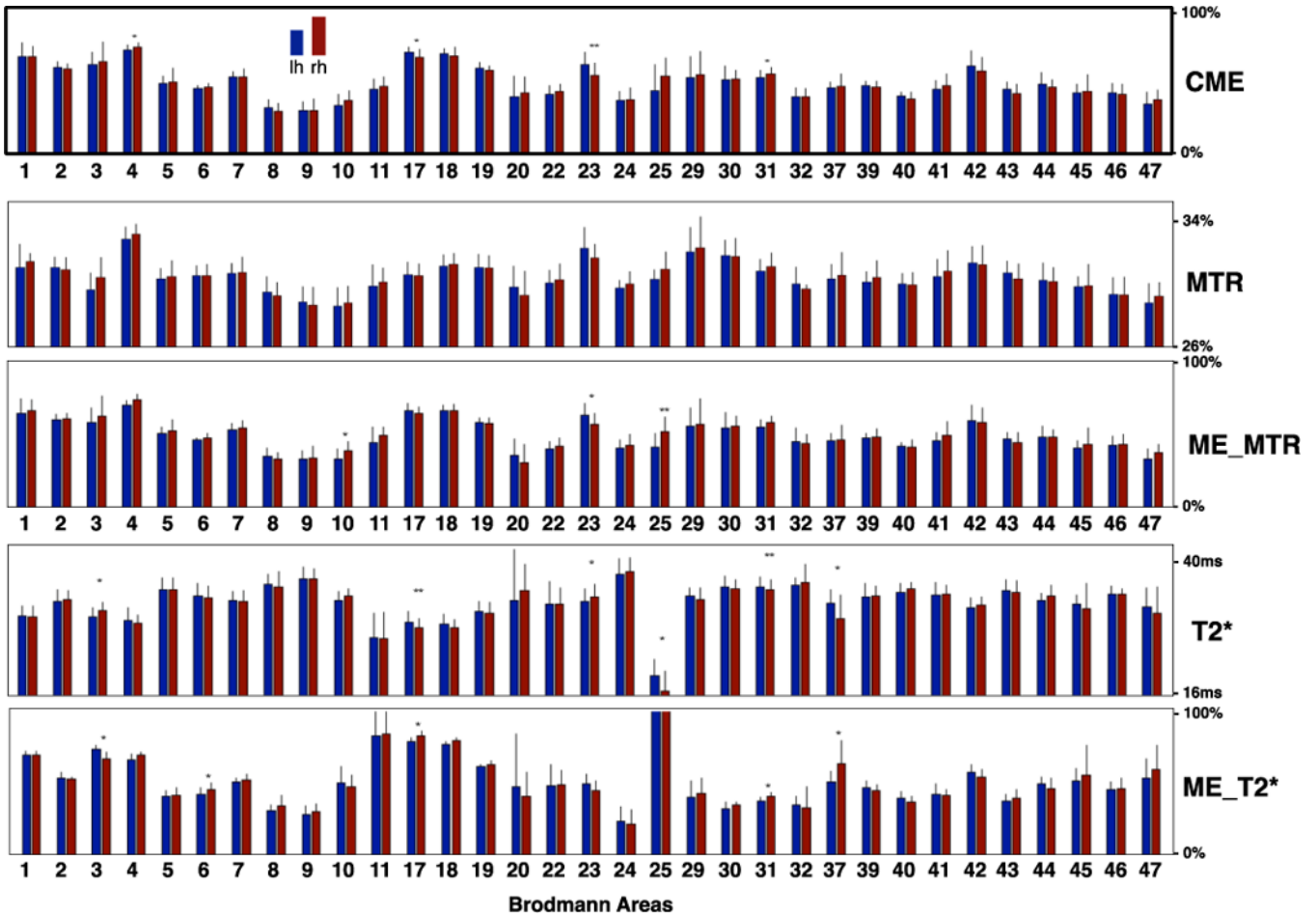


**Figure 10.**

Bar graphs representing mean and inter-subject SD values of the different metrics used in the MMEM (CME, MTR, ME\_MTR,  $T_2^*$ , ME\_  $T_2^*$ ) within Brodmann regions. Overall, we observe a fairly good right-left reproducibility. The CME map shows significant hemispheric differences in BA4 and BA31 (more myelin estimated in rh,  $p < 0.05$ ) and in BA17 and BA23 (more myelin estimated in lh, respectively  $p < 0.05$  and  $p < 0.01$ ).

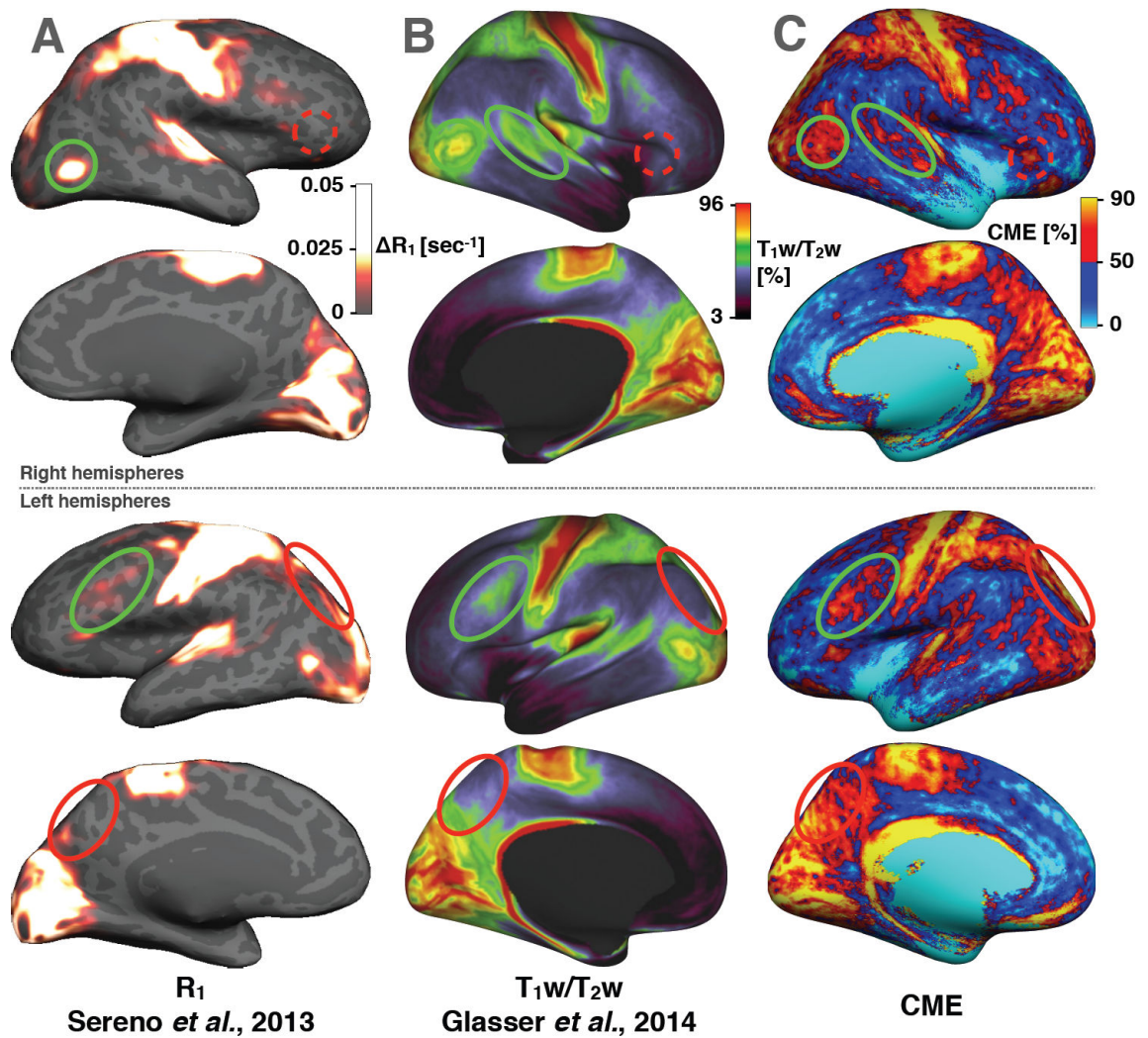


**Figure 11.**

Comparison with recent in vivo studies showing different contrasts sensitive to cortical myelin content in healthy adults. (A) quantitative  $R_1$  maps averaged across 6 control subjects (Sereno *et al.*, 2013).  $R_1$  is the difference between the mean  $R_1$  (across the cortex) and the  $R_1$  in a specific vertex. (B)  $T_1w/T_2w$  maps averaged across 69 subjects (Glasser and Van Essen, 2011). (C) CME maps averaged across 6 subjects, unsmoothed. Green circles show similarities between CME maps and  $R_1$  or  $T_1w/T_2w$ . Red circles show differences.

Mean, inter-subject SD and coefficient of variation (COV) of MTR,  $T_2^*$  and CT maps. Left and Right tables are showing results for left (LH) and right (RH) hemispheres respectively.

**Table 1**

LH	MTR [%]	$T_2^*$ [ms]	CT [mm]	RH	MTR [%]	$T_2^*$ [ms]	CT [mm]
Mean	31.04	32.16	2.61	Mean	31.02	32.03	2.60
SD	0.34	1.42	0.053	SD	0.41	1.39	0.061
COV [%]	1.1	4.4	2.0	COV [%]	1.3	4.3	2.3

Pearson's coefficient calculated vertex-wise between each pair of the following parameters: MTR, T<sub>2</sub>\*, CT and B0 orientation for left (LH) and right (RH) hemispheres.

**Table 2**

LH	Thickness	B0 orientation	RH	Thickness	B0 orientation
MTR	r = -0.19 p < 10 <sup>-16</sup>	r = 0.18 p < 10 <sup>-16</sup>	MTR	r = -0.24 p < 10 <sup>-16</sup>	r = 0.14 p < 10 <sup>-16</sup>
T <sub>2</sub> *	r = 0.52 p < 10 <sup>-16</sup>	r = -0.13 p < 10 <sup>-16</sup>	T <sub>2</sub> *	r = 0.42 p < 10 <sup>-16</sup>	r = -0.05 p < 10 <sup>-8</sup>

**Table 3**

Resulting coefficients of the linear models defined in equation 2,3 and their inter-subjects SD. Coefficients values are expressed in percentages in order to show their relatives contributions to the output maps (ME\_MTR and ME\_T<sub>2</sub>\*). *a* is the constant coefficient, *b* is the coefficient of the main metric (MTR in the ME\_MTR regression and T<sub>2</sub>\* in the ME\_T<sub>2</sub>\* regression), *c* is the CT coefficient, *d* and *e* are the coefficients of the B0 orientation dependency (see equations (2) and (3)).

	<i>a</i> [%]	<i>b</i> [%]	<i>c</i> [%]	<i>d</i> [%]	<i>e</i> [%]
ME_MTR	-39.1 ± 1.9	54.2 ± 0.4	-6.2 ± 1.7	-0.14 ± 0.4	-0.05 ± 0.13
ME_T <sub>2</sub> *	54.4 ± 2.0	-37.6 ± 2.9	-6.0 ± 2.5	0.33 ± 0.33	0.05 ± 0.12